

Four-Loop Vacuum Energy Density of the $SU(N_c)$ + Adjoint Higgs Theory

K. Kajantie^{a,1}, M. Laine^{b,2}, K. Rummukainen^{a,c,3}, Y. Schröder^{d,4}

^a*Department of Physics, P.O.Box 64, FIN-00014 University of Helsinki, Finland*

^b*Theory Division, CERN, CH-1211 Geneva 23, Switzerland*

^c*Helsinki Institute of Physics, P.O.Box 64, FIN-00014 University of Helsinki, Finland*

^d*Center for Theoretical Physics, MIT, Cambridge, MA 02139, USA*

We compute the dimensionally regularised four-loop vacuum energy density of the $SU(N_c)$ gauge + adjoint Higgs theory, in the disordered phase. “Scalarisation”, or reduction to a small set of master integrals of the type appearing in scalar field theories, is carried out in d dimensions, employing general partial integration identities through an algorithm developed by Laporta, while the remaining scalar integrals are evaluated in $d = 3 - 2\epsilon$ dimensions, by expanding in $\epsilon \ll 1$ and evaluating a number of coefficients. The results have implications for the thermodynamics of finite temperature QCD, allowing to determine perturbative contributions of orders $\mathcal{O}(g^6 \ln(1/g))$, $\mathcal{O}(g^6)$ to the pressure, while the general methods are applicable also to studies of critical phenomena in QED-like statistical physics systems.

April 2003

¹keijo.kajantie@helsinki.fi

²mikko.laine@cern.ch

³kari.rummukainen@helsinki.fi

⁴yorks@lns.mit.edu

1. Introduction

The theory we study in this paper is the Euclidean $SU(N_c)$ gauge + adjoint Higgs theory, defined in continuum dimensional regularisation by the action

$$S_E \equiv \int d^d x \mathcal{L}_E, \quad (1.1)$$

$$\mathcal{L}_E \equiv \frac{1}{2} \text{Tr} F_{kl}^2 + \text{Tr} [D_k, A_0]^2 + m^2 \text{Tr} A_0^2 + \lambda (\text{Tr} A_0^2)^2, \quad (1.2)$$

where $k, l = 1, \dots, d$, $D_k = \partial_k - igA_k$, $A_k = A_k^a T^a$, $A_0 = A_0^a T^a$, $F_{kl} = (i/g)[D_k, D_l]$, and T^a are the Hermitean generators of $SU(N_c)$, normalised as $\text{Tr} T^a T^b = \delta^{ab}/2$. Summation over repeated indices is understood. We could have taken the scalar potential also in the form $\lambda_1 (\text{Tr} A_0^2)^2 + \lambda_2 \text{Tr} A_0^4$, but the two quartic terms are independent only for $N_c \geq 4$ and thus, to avoid further proliferation of formulae, we will set $\lambda_2 = 0$ here, denoting $\lambda \equiv \lambda_1$. For the moment we keep d general, but later on we write $d = 3 - 2\epsilon$, and expand in $\epsilon \ll 1$.

The observable we would like to compute for the theory in Eq. (1.2) is its partition function, or “vacuum energy density”,

$$f(m^2, g^2, \lambda) \equiv - \lim_{V \rightarrow \infty} \frac{1}{V} \ln \int \mathcal{D}A_k \mathcal{D}A_0 \exp(-S_E). \quad (1.3)$$

Here V is the d -dimensional volume. The phase diagram of the system described by S_E has a “disordered”, or symmetric phase and, depending on N_c , various kinds of symmetry broken phases [1, 2]. Our aim is to determine the perturbative expansion for f up to 4-loop order in the symmetric phase, expanding around $A_0^a = A_k^a = 0$; the 3-loop result is known already [3, 4]. The result will depend on N_c through $d_A \equiv N_c^2 - 1$, $C_A \equiv N_c$.

The main motivation for the exercise described comes from finite temperature QCD. Indeed, the simplest physical observable there, the free energy density or minus the pressure, has been computed perturbatively up to resummed 3-loop level [5, 6], but the expansion converges very slowly, requiring probably temperatures $T \gg \text{TeV}$ to make any sense at all [5, 6, 3, 7]. Moreover, at the 4-loop level the expansion breaks down completely [8, 9]. Multiloop computations are not useless, though: these infrared problems can be isolated into the three-dimensional (3d) effective field theory in Eq. (1.2) [10], and studied non-perturbatively there with simple lattice simulations [4]. However, to convert the results from lattice regularisation to 3d continuum regularisation, and from the 3d continuum theory to the original 4d physical theory, still necessitates a number of perturbative multiloop “matching” computations.

The way our computation enters this setup has been described in [11]. Combining our results with those of another paper [12] allows one to determine, as explained in [11], all the logarithmic ultraviolet and infrared divergences entering the 4-loop free energy of QCD. This not only fixes the last perturbatively computable contribution to the free energy of hot QCD [11], of order $\mathcal{O}(g^6 \ln(1/g)T^4)$, but is also a step towards renormalising the non-perturbative contributions, as determined with lattice methods [4, 13]. Some other applications of our results are discussed in Sec. 8.

$$\begin{aligned}
\text{2-loop : } & \frac{1}{4} \text{ (circle with wavy line) } + \frac{1}{8} \text{ (two circles) } \\
\text{3-loop : } & \frac{1}{6} \text{ (circle with wavy line and ghost) } + \frac{1}{8} \text{ (circle with wavy line and ghost) } + \frac{1}{2} \text{ (circle with wavy line and ghost) } + \frac{1}{8} \text{ (circle with wavy line and ghost) } + \frac{1}{48} \text{ (two circles) } \\
\text{4-loop : } & -\frac{1}{3} \text{ (circle with wavy line and ghost) } + \frac{1}{4} \text{ (circle with wavy line and ghost) } + \frac{1}{4} \text{ (circle with wavy line and ghost) } + \frac{1}{2} \text{ (circle with wavy line and ghost) } + \frac{1}{6} \text{ (circle with wavy line and ghost) } + \frac{1}{12} \text{ (circle with wavy line and ghost) } \\
& + \frac{1}{2} \text{ (circle with wavy line and ghost) } + \frac{1}{2} \text{ (circle with wavy line and ghost) } + \frac{1}{2} \text{ (circle with wavy line and ghost) } + \frac{1}{8} \text{ (circle with wavy line and ghost) } + \frac{1}{4} \text{ (circle with wavy line and ghost) } + 1 \text{ (circle with wavy line and ghost) } + 1 \text{ (circle with wavy line and ghost) } \\
& + \frac{1}{4} \text{ (circle with wavy line and ghost) } + \frac{1}{8} \text{ (circle with wavy line and ghost) } + \frac{1}{2} \text{ (circle with wavy line and ghost) } + \frac{1}{2} \text{ (circle with wavy line and ghost) } + \frac{1}{8} \text{ (circle with wavy line and ghost) } + \frac{1}{2} \text{ (circle with wavy line and ghost) } \\
& + \frac{1}{2} \text{ (circle with wavy line and ghost) } + \frac{1}{16} \text{ (circle with wavy line and ghost) } + \frac{1}{6} \text{ (circle with wavy line and ghost) } + \frac{1}{4} \text{ (circle with wavy line and ghost) } + \frac{1}{4} \text{ (circle with wavy line and ghost) } + \frac{1}{16} \text{ (circle with wavy line and ghost) } + \frac{1}{8} \text{ (circle with wavy line and ghost) } + \frac{1}{48} \text{ (circle with wavy line and ghost) }
\end{aligned}$$

Figure 1: *The skeleton diagrams contributing in Eq. (1.3), after subtraction of those which obviously vanish because of colour contractions or specific properties of dimensional regularisation. Solid lines represent the adjoint scalar A_0 , wavy lines the gauge boson A_i , and dotted lines the ghosts. The complete sets of skeleton diagrams have been enumerated and written down in ref. [14], whose overall sign conventions we also follow.*

2. Outline of the general procedure

The first step of the perturbative computation is the generation of the Feynman diagrams. At 4-loop level, this is no longer a completely trivial task. In order to make the procedure tractable, we employ an algorithm whereby the graphs are generated in two sets: two-particle-irreducible “skeleton” graphs, as well as various types of “ring” diagrams, containing all possible self-energy insertions. The resulting sets, with the relevant symmetry factors, were provided explicitly in [14].

It actually turns out that some of the generic graphs shown in [14] do not contribute in the present computation. There are two reasons for this. First, once the Feynman rules for the interactions of gauge bosons and adjoint scalars are taken into account, some of the graphs vanish at the point of colour contractions. This concerns particularly the “non-planar” topologies [15]. Second, all vacuum graphs which do not contain at least one massive (adjoint scalar) line, vanish in strict dimensional regularisation. In some cases such a vanishing may be due to an unphysical cancellation between ultraviolet and infrared divergences, as we will recall in Sec. 7, but for the moment we accept the vanishing literally. The remaining skeleton graphs are then as shown in Fig. 1. For the ring diagrams, which by far outnumber the skeleton graphs, we find it simpler to treat the full sets as shown in [14], letting the two types of cancellations mentioned above come out automatically in the actual computation. For completeness, the ring diagrams are reproduced in Fig. 2.

The Feynman rules for the vertices and propagators appearing are the standard ones. We

$$\begin{aligned}
\text{wavy } \textcircled{1} &\equiv \frac{1}{2} \text{ (circular wavy) } - 1 \text{ (circular dashed) } + \frac{1}{2} \text{ (circular wavy with wavy bottom) } + \frac{1}{2} \text{ (circular) } + \frac{1}{2} \text{ (circular with wavy bottom) } , \\
\text{dashed } \textcircled{1} &\equiv 1 \text{ (circular dashed) } , \\
\text{solid } \textcircled{1} &\equiv 1 \text{ (circular) } + \frac{1}{2} \text{ (circular wavy) } + \frac{1}{2} \text{ (circular) } , \\
\text{wavy } \textcircled{2} &\equiv \frac{1}{2} \text{ (circular wavy) } - 1 \text{ (circular dashed) } - 1 \text{ (circular dashed with arrow) } - 1 \text{ (circular dashed with arrow) } + \frac{1}{2} \text{ (circular wavy) } + \frac{1}{2} \text{ (circular wavy) } \\
&\quad + \frac{1}{4} \text{ (two wavy circles) } + \frac{1}{6} \text{ (circular wavy) } + \frac{1}{2} \text{ (circular with vertical line) } + \frac{1}{2} \text{ (circular with vertical line) } + \frac{1}{2} \text{ (circular with vertical line) } \\
&\quad + 1 \text{ (circular with diagonal line) } + 1 \text{ (circular with diagonal line) } + \frac{1}{2} \text{ (circular with diagonal line) } + \frac{1}{2} \text{ (circular with diagonal line) } \\
&\quad + \frac{1}{4} \text{ (two circles) } + \frac{1}{4} \text{ (two circles) } + \frac{1}{2} \text{ (circular with wavy bottom) } + \frac{1}{4} \text{ (two circles) } , \\
\text{dashed } \textcircled{2} &\equiv 1 \text{ (circular dashed) } + 1 \text{ (circular dashed with arrow) } , \\
\text{solid } \textcircled{2} &\equiv 1 \text{ (circular) } + 1 \text{ (circular with vertical line) } + \frac{1}{2} \text{ (circular with diagonal line) } + \frac{1}{2} \text{ (circular with diagonal line) } + 1 \text{ (circular with diagonal line) } + 1 \text{ (circular with diagonal line) } \\
&\quad + 1 \text{ (two circles) } + \frac{1}{2} \text{ (circular with diagonal line) } + \frac{1}{2} \text{ (circular with diagonal line) } + \frac{1}{2} \text{ (circular with diagonal line) } + \frac{1}{6} \text{ (circular) } , \\
\text{wavy } \textcircled{2} &\equiv 1 \text{ (circular wavy) } - 1 \text{ (circular dashed) } - 1 \text{ (circular dashed with arrow) } + \frac{1}{2} \text{ (circular wavy) } + 1 \text{ (circular) } + \frac{1}{2} \text{ (circular) } , \\
\text{dashed } \textcircled{2} &\equiv 1 \text{ (circular dashed) } + 1 \text{ (circular dashed with arrow) } , \\
\text{solid } \textcircled{2} &\equiv 1 \text{ (circular) } + 1 \text{ (circular with wavy bottom) } + \frac{1}{2} \text{ (circular wavy) } + \frac{1}{2} \text{ (circular) } , \\
\text{3-loop:} &\quad \frac{1}{4} \text{ (two circles) } - \frac{1}{2} \text{ (two circles) } + \frac{1}{4} \text{ (two circles) } , \\
\text{4-loop:} &\quad \frac{1}{6} \text{ (two circles) } + \frac{1}{2} \text{ (two circles) } + \frac{1}{4} \text{ (two circles) } - \frac{1}{3} \text{ (two circles) } - 1 \text{ (two circles) } - \frac{1}{2} \text{ (two circles) } \\
&\quad + \frac{1}{6} \text{ (two circles) } + \frac{1}{2} \text{ (two circles) } + \frac{1}{4} \text{ (two circles) } .
\end{aligned}$$

Figure 2: The ring diagrams contributing in Eq. (1.3) [14]. The notation is as in Fig. 1.

employ covariant gauge fixing, with a general gauge fixing parameter, denoted here by

$$\xi \equiv \xi_{\text{here}} \equiv 1 - \xi_{\text{standard}} , \quad (2.1)$$

where ξ_{standard} is the gauge fixing parameter of the standard covariant gauges. Therefore, Feynman gauge corresponds here to $\xi = 0$, Landau gauge to $\xi = 1$. We keep everywhere ξ completely general, however, and verify explicitly that it cancels in all the results.

The graphs having been identified and the Feynman rules specified, we program them [16] in the symbolic manipulation package FORM [17], for further treatment.

After the colour contractions, the next step is to “scalarise” the remaining integrals. That is, we want to remove all scalar products from the numerators of the momentum integrations, such that only integrations of the type appearing in scalar field theories remain. This problem can be solved by using general partial integration identities [18]. The full power of the identities can be conveniently made use of through an algorithm developed by Laporta [19]. We discuss some aspects of our implementation of this algorithm, together with the results obtained, in Sec. 3.

After the reduction to scalar integrals, we are faced with their evaluation. At this point one has to specify the dimension d of the spacetime, in order to make further progress. We write $d = 3 - 2\epsilon$, expand in $\epsilon \ll 1$, and evaluate the various scalar integrals appearing to a certain (integral-dependent) depth in this expansion, such that a specified order is achieved for the overall result. For the new 4-loop contributions, the overall order for which we have either analytic or numerical expressions is $\mathcal{O}(1)$. The scalar integrals needed for this are discussed in Sec. 4.

There is one remaining step to be taken before we have the final result: the renormalisation of the parameters m^2, g^2, λ in Eq. (1.2). In other words, the results presented up to this point were in terms of the bare parameters, and we now want to re-expand them in terms of the renormalised parameters. This step is also specific to the dimension, and turns out to be particularly simple for $d = 3 - 2\epsilon$, since only the mass parameter gets renormalised. The conversion of the bare parameters to the renormalised ones is discussed in Sec. 5, and the final form of the results is then shown in Sec. 6.

Having completed the straightforward computation, we discuss the conceptual issue of infrared divergences in Sec. 7. We mention in this context also some checks of our results, based on largely independent computations. We end with a list of some applications in Sec. 8.

3. Scalarisation in d dimensions

After inserting the Feynman rules and carrying out the colour contractions, there remains, at 4-loop level, a $4d$ -dimensional momentum integration to be carried out. The different types of integrations emerging can be illustrated in graphical notation in the standard way. Without specifying the fairly complicated numerators, involving all possible kinds of scalar products of the integration momenta, the graphs are of the general types shown in Fig. 3.

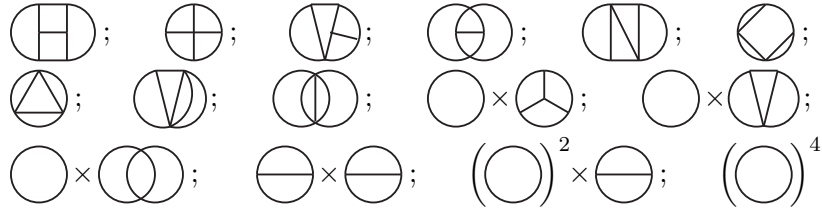


Figure 3: *The 15 general types of 4-loop integrations remaining, in terms of momentum flow (momentum conservation is assumed at the vertices), after taking into account that colour contractions remove the non-planar topologies. Any line could contain a propagator to some power $n \geq 1$, and there is also an unspecified collection of scalar products of the integration momenta in the numerator.*

There are a few simple tricks available in order to try and simplify the scalar products appearing in the numerators [16]. For instance, one can find relabelings of the integration variables such that the denominators appearing in the graph remain the same, while the scalar products in the numerators may get simplified, after symmetrising between such relabelings. Some scalar products in the numerators can also be completed into sums of squares, such that they cancel against the denominators. Furthermore, we can make use of various special properties of dimensional regularisation: any closed massless 1-loop tadpole integral vanishes; and any 1-loop massive bubble diagram with at most one external momentum is easily scalarised explicitly, in the sense of removing the loop momentum from all the scalar products appearing in the numerators. However, while such simple tricks are sufficient at, say, 2-loop level, this is no longer the case at 4-loop level.

To scalarise the 4-loop integrations, we have to make full use of the identities provided by general partial integrations [18]. To systematically employ all such identities, we implement the algorithm presented by Laporta [19] using the “tables” routines of FORM [17]. This leads to a complete solution of our problem. The main technical details of our implementation were discussed in [16].

After the scalarisation, the master integrals remaining are those shown in Fig. 4. This basis is, of course, not unique. As an example, one could have chosen a different basis for the 3-loop master integrals, employing identities following from partial integrations [20],

$$\text{Two overlapping circles} = \frac{1}{m^2} \left(\text{Circle} \right)^3 \left[-\frac{(d-2)^2}{(d-3)(3d-8)} \right] + m^2 \text{Circle with vertical line} \left[\frac{4(d-3)}{(3d-8)} \right], \quad (3.1)$$

$$\text{Two overlapping circles} = \frac{1}{m^2} \left(\text{Circle} \right)^3 \left[-\frac{2(d-2)^2}{(d-3)(3d-8)} \right] + m^2 \text{Circle with vertical line} \left[-\frac{4(d-4)}{(3d-8)} \right], \quad (3.2)$$

where

$$\text{Circle} \equiv \int \frac{d^d p}{(2\pi)^d} \frac{1}{p^2 + m^2}, \quad (3.3)$$

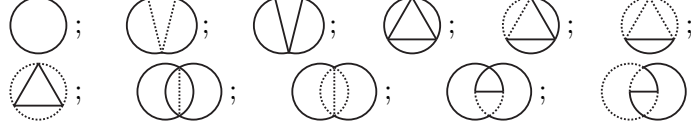


Figure 4: *The 1-loop, 3-loop and 4-loop “master” topologies remaining after “scalarisation”. There are no numerators left in these graphs. A solid line is a massive propagator, $1/(p^2 + m^2)$, and a dotted line a massless one, $1/p^2$, where p is the Euclidean momentum flowing through the line. Note that no independent 2-loop representative appears.*

and correspondingly for the higher loop integrals. Therefore, the 3-loop master integrals we are using, appearing on the right-hand-sides of Eqs. (3.1), (3.2), could be exchanged in favour of the 3-loop integrals on the left-hand-sides of Eqs. (3.1), (3.2).

To display the full result after scalarisation, we introduce the shorthand notations

$$f(m^2, g^2, \lambda) \equiv -d_A \sum_{\ell=1}^{\infty} (g^2 C_A)^{\ell-1} \hat{p}_\ell, \quad \bar{\lambda} \equiv \frac{\lambda(d_A + 2)}{g^2 C_A}. \quad (3.4)$$

We then obtain the following expressions:

$$\hat{p}_1 = m^2 \left(\bigcirc \right) \left[-\frac{1}{d} \right], \quad (3.5)$$

$$\hat{p}_2 = \left(\bigcirc \right)^2 \left[\frac{(d-1)}{4(d-3)} - \frac{1}{4} \bar{\lambda} \right], \quad (3.6)$$

$$\begin{aligned} \hat{p}_3 = & \frac{1}{m^2} \left(\bigcirc \right)^3 \times \\ & \times \left\{ \left[-\frac{(d-2)(608 - 1064d + 654d^2 - 155d^3 + 12d^4)}{8(d-6)(d-4)(2d-7)(3d-8)} \right] + \right. \\ & + \bar{\lambda} \left[\frac{(d-2)(d-1)}{4(d-3)} \right] + \\ & \left. + \bar{\lambda}^2 \left[-\frac{(d-2)}{8} - \frac{(d-2)^2}{2(d_A+2)(d-3)(3d-8)} \right] \right\} + \\ & + m^2 \left(\bigcirc \right) \left[\frac{(d-2)^3(3d-11)}{(d-4)(2d-7)(3d-8)} \right] + \\ & + m^2 \left(\bigcirc \right) \left[-\frac{(16 - 18d + 3d^2)}{2(d-6)(d-4)(3d-8)} - \bar{\lambda}^2 \frac{(d-4)}{(d_A+2)(3d-8)} \right], \quad (3.7) \end{aligned}$$

$$\begin{aligned} \hat{p}_4 = & \frac{1}{m^4} \left(\bigcirc \right)^4 \times \\ & \times \left\{ \frac{(d-2)\alpha_1}{96(d-9)(d-7)(d-6)(d-5)(d-4)^2(d-3)^3} \times \right. \\ & \left. \times \frac{1}{(d-1)(2d-9)(2d-7)(3d-13)(3d-11)(3d-10)(3d-8)} \right\} + \end{aligned}$$

$$\begin{aligned}
& +\bar{\lambda} \left[-\frac{(d-2)(2904 - 7150d + 7097d^2 - 3581d^3 + 964d^4 - 131d^5 + 7d^6)}{8(d-6)(d-4)(d-3)^2(2d-7)} - \right. \\
& \quad \left. -\frac{5(d-5)(d-2)^3}{4(d_A+2)(d-4)^2(d-3)(3d-11)} \right] + \\
& +\bar{\lambda}^2 \left[\frac{(d-2)(d-1)(2d-5)}{8(d-3)} + \frac{(d-2)^2(-32 + 56d - 25d^2 + 3d^3)}{4(d_A+2)(d-4)(d-3)^2(3d-8)} \right] + \\
& +\bar{\lambda}^3 \left[-\frac{(d-2)(2d-5)}{24} - \frac{(d-2)^2}{4(d_A+2)(d-3)} \right] \Big\} + \\
& + \left(\bigcirc \right) \times \left(\bigcirc \text{ with } \nabla \right) \times \\
& \times \left\{ \left[-\frac{(d-2)^2\alpha_2}{24(d-5)(d-4)^2(d-3)(d-1)(2d-9)(2d-7)(3d-11)(3d-10)(3d-8)} \right] + \right. \\
& \left. +\bar{\lambda} \left[\frac{(d-2)^3(3d-11)}{2(d-4)(2d-7)} \right] \right\} + \\
& + \left(\bigcirc \right) \times \left(\bigcirc \text{ with } \nabla \right) \times \\
& \times \left\{ \frac{\alpha_3}{24(d-9)(d-7)(d-6)(d-5)(d-4)(d-3)} \times \right. \\
& \quad \left. \times \frac{1}{(d-1)(2d-9)(3d-13)(3d-11)(3d-8)} + \right. \\
& \left. +\bar{\lambda} \left[-\frac{16 - 18d + 3d^2}{4(d-6)(d-4)} - \frac{5(d-6)(d-2)}{(d_A+2)(d-4)(3d-11)} \right] + \right. \\
& \left. +\bar{\lambda}^2 \left[\frac{-32 + 56d - 25d^2 + 3d^3}{2(d_A+2)(d-3)(3d-8)} \right] + \right. \\
& \left. +\bar{\lambda}^3 \left[-\frac{(d-4)}{2(d_A+2)} \right] \right\} + \\
& + \left(\bigcirc \text{ with } \triangle \right) \times \\
& \times \left\{ \frac{\alpha_4}{144(d-9)(d-7)(d-5)(d-4)^2(d-1)(3d-13)(3d-11)} + \right. \\
& \left. +\bar{\lambda} \left[-\frac{5(96 - 64d + 7d^2 + d^3)}{12(d_A+2)(d-4)^2(3d-11)} \right] + \right. \\
& \left. +\bar{\lambda}^2 \left[\frac{d}{6(d_A+2)(d-4)} \right] + \right. \\
& \left. +\bar{\lambda}^3 \left[-\frac{(d_A+8)}{6(d_A+2)^2} \right] \right\} + \\
& + \left(\bigcirc \text{ with } \triangle \text{ and } \nabla \right) \times \\
& \times \left\{ \left[-\frac{8136 - 18176d + 14438d^2 - 5370d^3 + 984d^4 - 81d^5 + 2d^6}{16(d-5)(d-4)^2(d-1)(2d-9)} \right] + \right.
\end{aligned}$$

$$\begin{aligned}
& + \bar{\lambda} \left[-\frac{5(20 - 10d + d^2)}{4(d_A + 2)(d - 4)} \right] \Big\} + \\
& + \text{[Diagram: Triangle with a horizontal line through the middle]} \left[-\frac{(d - 2)(-2656 + 5672d - 4072d^2 + 1302d^3 - 186d^4 + 9d^5)}{16(d - 4)(d - 1)(3d - 11)(3d - 10)} \right] + \\
& + \text{[Diagram: Triangle with a vertical line through the middle]} \left[-\frac{4(d - 2)(-9482 + 13225d - 7306d^2 + 1992d^3 - 267d^4 + 14d^5)}{9(d - 4)^2(2d - 7)(3d - 11)(3d - 10)} \right] + \\
& + \frac{1}{m^2} \text{[Diagram: Two overlapping circles]} \times \\
& \quad \times \left\{ \left[-\frac{(d - 2)(2d - 5)\alpha_5}{24(d - 4)^2(d - 3)(d - 1)(2d - 9)(2d - 7)} \right] + \right. \\
& \quad \left. + \bar{\lambda}^2 \left[-\frac{(d - 2)(2d - 5)}{2(d_A + 2)(d - 4)(d - 3)} \right] \right\} + \\
& + \frac{1}{m^2} \text{[Diagram: Two overlapping circles]} \left[\frac{(d - 2)(2d - 5)\alpha_6}{3(d - 4)^3(d - 3)^2(d - 1)(2d - 7)(3d - 11)(3d - 10)} \right] + \\
& + m^2 \text{[Diagram: Two overlapping circles]} \left\{ \left[-\frac{3(11 - 7d + d^2)}{(d - 4)(2d - 9)} \right] + \bar{\lambda} \left[-\frac{10(d - 3)}{(d_A + 2)(d - 4)} \right] \right\} + \\
& + m^2 \text{[Diagram: Two overlapping circles]} \left[\frac{2(d - 3)(d - 2)}{(d - 4)(2d - 7)} \right], \tag{3.8}
\end{aligned}$$

where

$$\begin{aligned}
\alpha_1 = & -121583669760 + 2691971008704d - 13463496742176d^2 + 33122892972480d^3 - \\
& -50028680189824d^4 + 51445267135192d^5 - 38155599595406d^6 + 21131958532365d^7 - \\
& -8925676618775d^8 + 2909006141441d^9 - 734705333783d^{10} + 143430052519d^{11} - \\
& -21428725861d^{12} + 2402935979d^{13} - 195570319d^{14} + \\
& + 10896768d^{15} - 371376d^{16} + 5832d^{17}, \tag{3.9}
\end{aligned}$$

$$\begin{aligned}
\alpha_2 = & -14081760 + 11237380d + 64451424d^2 - 140115669d^3 + 129957772d^4 - \\
& -69456108d^5 + 23323366d^6 - 5020699d^7 + 674926d^8 - 51720d^9 + 1728d^{10}, \tag{3.10}
\end{aligned}$$

$$\begin{aligned}
\alpha_3 = & 508742208 - 1725645240d + 2236030380d^2 - 1426818168d^3 + \\
& + 436152106d^4 - 14158652d^5 - 36636937d^6 + 13713052d^7 - \\
& -2491870d^8 + 254770d^9 - 13967d^{10} + 318d^{11}, \tag{3.11}
\end{aligned}$$

$$\begin{aligned}
\alpha_4 = & -1266048 - 122112d + 1785942d^2 - 1171982d^3 + \\
& + 307185d^4 - 35512d^5 + 1400d^6 + 6d^7 + d^8, \tag{3.12}
\end{aligned}$$

$$\alpha_5 = 5112 - 11321d + 10618d^2 - 5358d^3 + 1489d^4 - 212d^5 + 12d^6, \tag{3.13}$$

$$\begin{aligned}
\alpha_6 = & 171232 - 492404d + 584218d^2 - 380046d^3 + \\
& + 149811d^4 - 36924d^5 + 5595d^6 - 480d^7 + 18d^8. \tag{3.14}
\end{aligned}$$

It is worth stressing that Eqs. (3.5)–(3.14) were obtained with an arbitrary ξ , which just exactly cancelled once all the graphs were summed together, for a general d , and before

inserting any properties of the master integrals. This is a consequence of the fact that the master integrals constitute really a linearly independent basis for the present problem.

4. Integrals in $d = 3 - 2\epsilon$ dimensions

A set of master scalar integrals having been identified, the next step is to compute them. As already mentioned, we do this by writing $d = 3 - 2\epsilon$, expanding in $\epsilon \ll 1$, and evaluating a number of coefficients in the series.

In order to display the results, we first choose a convenient integration measure. To this end, we introduce an $\overline{\text{MS}}$ scale parameter $\bar{\mu}$, by writing each integration as

$$\int \frac{d^d p}{(2\pi)^d} \equiv \mu^{-2\epsilon} \left[\bar{\mu}^{2\epsilon} \left(\frac{e^\gamma}{4\pi} \right)^\epsilon \int \frac{d^d p}{(2\pi)^d} \right], \quad (4.1)$$

where $\mu = \bar{\mu}(e^\gamma/4\pi)^{1/2}$, and the expression in square brackets has integer dimensionality. This square bracket part of an ℓ -loop integration is then written as

$$\begin{aligned} & \left[\prod_{i=1}^{\ell} \left\{ \bar{\mu}^{2\epsilon} \left(\frac{e^\gamma}{4\pi} \right)^\epsilon \int \frac{d^d p_i}{(2\pi)^d} \right\} \right] g(p_1, \dots, p_\ell, m) = \\ & = \frac{1}{(4\pi)^\ell} m^{3\ell-2k} \left(\frac{\bar{\mu}}{2m} \right)^{2\epsilon\ell} \left\{ \prod_{i=1}^{\ell} \left[4\pi \left(\frac{e^\gamma}{\pi} \right)^\epsilon \int \frac{d^{3-2\epsilon} p_i}{(2\pi)^{3-2\epsilon}} \right] g(p_1, \dots, p_\ell, 1) \right\}, \end{aligned} \quad (4.2)$$

where k counts the number of propagators, or lines, in the graphical representation of the function g . From now on we assume that the loop integrations are computed with the dimensionless measure in the curly brackets in Eq. (4.2), while the constants in front of the curly brackets, together with the explicit powers of m as they appear in Eqs. (3.5)–(3.8), are to be provided in trivial prefactors (cf. Eq. (4.14) below).

With such conventions, the loop integrals remaining are functions of ϵ only, and read:

$$\textcircled{\quad} = -1 - 2\epsilon - \epsilon^2 \left(4 + \frac{1}{4} \pi^2 \right) + \epsilon^3 \gamma_1 + \mathcal{O}(\epsilon^4), \quad (4.3)$$

$$\textcircled{\text{V}} = \frac{\pi^2}{12} + \epsilon \gamma_2 + \mathcal{O}(\epsilon^2), \quad (4.4)$$

$$\textcircled{\text{V}} = \ln 2 + \epsilon \gamma_3 + \mathcal{O}(\epsilon^2), \quad (4.5)$$

$$\textcircled{\text{A}} = \frac{\pi^2}{32\epsilon} + \gamma_4 + \mathcal{O}(\epsilon), \quad (4.6)$$

$$\textcircled{\text{A}} = \frac{\pi^2}{32\epsilon} + \gamma_5 + \mathcal{O}(\epsilon), \quad (4.7)$$

$$\textcircled{\text{A}} = \frac{\pi^2}{32\epsilon} + \gamma_6 + \mathcal{O}(\epsilon), \quad (4.8)$$

$$\textcircled{\text{A}} = \frac{\pi^2}{32\epsilon} + \gamma_7 + \mathcal{O}(\epsilon), \quad (4.9)$$

$$\begin{array}{c} \text{Diagram 1} \\ \text{Diagram 2} \\ \text{Diagram 3} \\ \text{Diagram 4} \end{array} = \begin{array}{l} \frac{7}{4\epsilon} - 8 \ln 2 + 21 + \epsilon \gamma_8 + \mathcal{O}(\epsilon^2), \\ \frac{3}{8\epsilon} + \frac{9}{2} + \epsilon \left(\frac{75}{2} + \frac{11}{8} \pi^2 \right) + \epsilon^2 \gamma_9 + \mathcal{O}(\epsilon^3), \\ \gamma_{10} + \mathcal{O}(\epsilon), \\ \mathcal{O}(1). \end{array} \quad (4.10)$$

$$\begin{array}{c} \text{Diagram 1} \\ \text{Diagram 2} \\ \text{Diagram 3} \\ \text{Diagram 4} \end{array} = \begin{array}{l} \frac{3}{8\epsilon} + \frac{9}{2} + \epsilon \left(\frac{75}{2} + \frac{11}{8} \pi^2 \right) + \epsilon^2 \gamma_9 + \mathcal{O}(\epsilon^3), \\ \gamma_{10} + \mathcal{O}(\epsilon), \\ \mathcal{O}(1). \end{array} \quad (4.11)$$

$$\begin{array}{c} \text{Diagram 1} \\ \text{Diagram 2} \\ \text{Diagram 3} \\ \text{Diagram 4} \end{array} = \begin{array}{l} \gamma_{10} + \mathcal{O}(\epsilon), \\ \mathcal{O}(1). \end{array} \quad (4.12)$$

$$\begin{array}{c} \text{Diagram 1} \\ \text{Diagram 2} \\ \text{Diagram 3} \\ \text{Diagram 4} \end{array} = \begin{array}{l} \mathcal{O}(1). \end{array} \quad (4.13)$$

As we will see, the terms shown explicitly are needed for determining the $1/\epsilon$ -poles in the 4-loop expression for f , the constants γ_n are needed for determining the finite 4-loop contribution to f , and the higher order terms only contribute at the level $\mathcal{O}(\epsilon)$. Analytic results for $\gamma_1, \dots, \gamma_9$, as well as a numerical determination of γ_{10} , are presented in Appendix A.

It is now convenient to combine the conventions in Eqs. (3.4), (4.1), (4.2) and write

$$f(m^2, g^2, \lambda) = -d_A \frac{\mu^{-2\epsilon}}{4\pi} \sum_{\ell=1}^{\infty} m^{4-\ell} \left(\frac{\bar{\mu}}{2m} \right)^{2\ell} \left(\frac{\mu^{-2\epsilon} g^2 C_A}{4\pi} \right)^{\ell-1} \tilde{p}_\ell. \quad (4.14)$$

Substituting Eqs. (4.3)–(4.13) into Eqs. (3.5)–(3.8) and expanding in ϵ , the results then read, up to $\mathcal{O}(\epsilon)$ corrections:

$$\tilde{p}_1 = +\frac{1}{3}, \quad (4.15)$$

$$\tilde{p}_2 = -\frac{1}{4} \left(\frac{1}{\epsilon} + 3 + \bar{\lambda} \right), \quad (4.16)$$

$$\begin{aligned} \tilde{p}_3 = & -\frac{89}{24} + \frac{11}{6} \ln 2 - \frac{1}{6} \pi^2 + \\ & + \frac{\bar{\lambda}}{4} \left(\frac{1}{\epsilon} + 3 \right) + \frac{\bar{\lambda}^2}{4} \left[\frac{1}{2} - \frac{1}{d_A + 2} \left(\frac{1}{\epsilon} + 8 - 4 \ln 2 \right) \right], \end{aligned} \quad (4.17)$$

$$\begin{aligned} \tilde{p}_4 = & +\frac{1}{\epsilon} \left(\frac{43}{32} - \frac{491}{6144} \pi^2 \right) + \frac{85291}{768} - \frac{1259}{32} \ln 2 + \frac{5653}{1536} \pi^2 - \\ & -\frac{1}{4} \gamma_1 + \frac{5}{3} \gamma_2 - \frac{19}{6} \gamma_3 - \frac{157}{192} \gamma_4 - \frac{13}{64} (\gamma_5 + \gamma_6) - \frac{4}{9} \gamma_7 - \frac{19}{48} \gamma_8 - \frac{1}{6} \gamma_9 + \gamma_{10} + \\ & + \bar{\lambda} \left[-\frac{1}{16\epsilon^2} - \frac{1}{8\epsilon} \left(1 + \frac{5}{(d_A + 2)} \left(\frac{\pi^2}{8} - 1 \right) \right) + \right. \\ & \left. + \frac{37}{24} - \frac{11}{12} \ln 2 + \frac{\pi^2}{48} + \frac{1}{d_A + 2} \left(-\frac{5}{2} - \frac{15}{2} \ln 2 + \frac{115}{192} \pi^2 - \frac{5}{4} (\gamma_4 + \gamma_5) \right) \right] + \\ & + \bar{\lambda}^2 \left[\frac{1}{16\epsilon^2} \frac{1}{d_A + 2} - \frac{1}{8\epsilon} \left(1 + \frac{1}{d_A + 2} \left(\frac{\pi^2}{8} - 5 \right) \right) - \right. \\ & \left. - \frac{1}{8} + \frac{1}{d_A + 2} \left(46 - \frac{51}{2} \ln 2 + \frac{13}{24} \pi^2 - 2\gamma_3 - \frac{1}{2} \gamma_4 - \frac{1}{4} \gamma_8 \right) \right] + \\ & + \bar{\lambda}^3 \left[\frac{1}{\epsilon} \left(\frac{1}{8} \frac{1}{d_A + 2} - \frac{\pi^2}{192} \frac{(d_A + 8)}{(d_A + 2)^2} \right) - \right. \\ & \left. - \frac{1}{24} + \frac{1}{2(d_A + 2)} (1 - \ln 2) - \frac{1}{6} \frac{(d_A + 8)}{(d_A + 2)^2} \gamma_4 \right]. \end{aligned} \quad (4.18)$$

It is interesting to note that while single diagrams contributing to \tilde{p}_3 do have $1/\epsilon$ -poles (cf. Appendix B), they sum to zero in the term without $\bar{\lambda}$, but not in the terms proportional to $\bar{\lambda}, \bar{\lambda}^2$. This structure is related to counterterm contributions from lower orders, as discussed in the next section. Similarly, single diagrams contributing to \tilde{p}_4 have both $1/\epsilon^2$ and $1/\epsilon$ -poles, but the former ones sum to zero in the term without any $\bar{\lambda}$'s.

Of course, single diagrams contain also ξ -dependence. In our computation ξ cancelled at the stage of Eqs. (3.5)–(3.14), but one could alternatively express single diagrams in terms of the same basis of master integrals, this time with ξ -dependent coefficients, and let the ξ 's sum to zero only in the end. For completeness, we again illustrate the general structure of such expressions at the 3-loop level, in Appendix B.

5. Counterterm contributions

The computation so far has been in terms of the bare parameters of the Lagrangian in Eq. (1.2). As a final step the result is, however, to be converted into an expansion in terms of the renormalised parameters.

The conversion is particularly simple in low dimensions such as close to $d = 3$, since then the theory in Eq. (1.2) is super-renormalisable. In fact, the only parameter requiring renormalisation is the mass parameter m^2 . We write it as

$$m^2 \equiv m_{\text{bare}}^2 = m^2(\bar{\mu}) + \delta m^2, \quad (5.1)$$

$$\delta m^2 = 2(d_A + 2) \frac{1}{(4\pi)^2} \frac{\mu^{-4\epsilon}}{4\epsilon} \left(-g^2 \lambda C_A + \lambda^2 \right). \quad (5.2)$$

This exact counterterm [21, 22] guarantees that all n -point Green's functions computed with the theory are ultraviolet finite. Note that as far as dimensional reasons and single diagrams are concerned, there could also be divergences of the form g^4/ϵ , but they sum to zero in the counterterm appearing in Eq. (5.2).

Inserting now Eqs. (5.1), (5.2) into the 1-loop and 2-loop expressions for $f(m^2, g^2, \lambda)$, we get contributions of the same order as the 3-loop and 4-loop vacuum graphs, respectively, from $\delta m^2 \cdot \partial_{m^2} f(m^2(\bar{\mu}), g^2, \lambda)$. We need to use here Eqs. (3.5), (3.6), since $\mathcal{O}(\epsilon)$ -terms, not shown in Eqs. (4.15), (4.16), contribute as well, being multiplied by the $1/\epsilon$ in δm^2 . Explicitly, the terms to be added to Eqs. (4.17), (4.18), once the prefactors in Eq. (4.14) are expressed in terms of the renormalised parameter $m(\bar{\mu})$ rather than m , are

$$\delta \tilde{p}_3 = \left(\frac{\bar{\mu}}{2m(\bar{\mu})} \right)^{-4\epsilon} \left(\frac{1}{4\epsilon} + \frac{1}{2} \right) \left(-\bar{\lambda} + \frac{1}{d_A + 2} \bar{\lambda}^2 \right), \quad (5.3)$$

$$\delta \tilde{p}_4 = \left(\frac{\bar{\mu}}{2m(\bar{\mu})} \right)^{-4\epsilon} \left(-\frac{1}{8} \right) \left(\frac{1}{\epsilon^2} + \frac{1}{\epsilon} (1 + \bar{\lambda}) + \frac{1}{2} (4 + \pi^2) + 2\bar{\lambda} \right) \left(-\bar{\lambda} + \frac{1}{d_A + 2} \bar{\lambda}^2 \right). \quad (5.4)$$

The 3-loop $1/\epsilon$ -contributions in Eq. (5.3) cancel against the $1/\epsilon$ -terms in Eq. (4.17). Indeed, genuine vacuum divergences can only appear in \tilde{p}_2, \tilde{p}_4 , since such divergences must be analytic

in the parameters m^2, g^2, λ appearing in the Lagrangian, while \tilde{p}_3 comes with a coefficient $\sim (m^2(\bar{\mu}))^{1/2}$ (cf. Eq. (4.14)). Another point to note is that $1/\epsilon^2$ -terms appear in $\delta\tilde{p}_4$ only with coefficients $\bar{\lambda}, \bar{\lambda}^2$, just as in Eq. (4.18), although there is no complete cancellation.

6. The final result

We can now collect together the full result for $f(m^2, g^2, \lambda)$, in terms of the renormalised parameters of the theory. For dimensional reasons, its structure is,

$$\begin{aligned}
f(m^2, g^2, \lambda) &= \frac{\mu^{-2\epsilon}}{4\pi} [\tilde{f}_{1,0}] m^3(\bar{\mu}) + \\
&+ \frac{\mu^{-4\epsilon}}{(4\pi)^2} [\tilde{f}_{2,0} g^2 + \tilde{f}_{2,1} \lambda] m^2(\bar{\mu}) + \\
&+ \frac{\mu^{-6\epsilon}}{(4\pi)^3} [\tilde{f}_{3,0} g^4 + \tilde{f}_{3,1} g^2 \lambda + \tilde{f}_{3,2} \lambda^2] m(\bar{\mu}) + \\
&+ \frac{\mu^{-8\epsilon}}{(4\pi)^4} [\tilde{f}_{4,0} g^6 + \tilde{f}_{4,1} g^4 \lambda + \tilde{f}_{4,2} g^2 \lambda^2 + \tilde{f}_{4,3} \lambda^3] + \dots, \tag{6.1}
\end{aligned}$$

where $\tilde{f}_{\ell,i} = \tilde{f}_{\ell,i}(\epsilon, \bar{\mu}/m(\bar{\mu}))$ are dimensionless numbers, with ℓ indicating the loop order, and i the number of λ 's appearing:

$$\tilde{f}_{1,0} = d_A \left(-\frac{1}{3} + \mathcal{O}(\epsilon) \right), \tag{6.2}$$

$$\tilde{f}_{2,0} = d_A C_A \left(\frac{1}{4\epsilon} + \ln \frac{\bar{\mu}}{2m(\bar{\mu})} + \frac{3}{4} + \mathcal{O}(\epsilon) \right), \tag{6.3}$$

$$\tilde{f}_{2,1} = d_A (d_A + 2) \left(\frac{1}{4} + \mathcal{O}(\epsilon) \right), \tag{6.4}$$

$$\tilde{f}_{3,0} = d_A C_A^2 \left(\frac{89}{24} - \frac{11}{6} \ln 2 + \frac{\pi^2}{6} + \mathcal{O}(\epsilon) \right), \tag{6.5}$$

$$\tilde{f}_{3,1} = d_A C_A (d_A + 2) \left(-\ln \frac{\bar{\mu}}{2m(\bar{\mu})} - \frac{1}{4} + \mathcal{O}(\epsilon) \right), \tag{6.6}$$

$$\begin{aligned}
\tilde{f}_{3,2} &= d_A (d_A + 2) \left(\ln \frac{\bar{\mu}}{2m(\bar{\mu})} + \frac{3}{2} - \ln 2 + \mathcal{O}(\epsilon) \right) + \\
&+ d_A (d_A + 2)^2 \left(-\frac{1}{8} + \mathcal{O}(\epsilon) \right), \tag{6.7}
\end{aligned}$$

$$\begin{aligned}
\tilde{f}_{4,0} &= d_A C_A^3 \left[\left(\frac{43}{32} - \frac{491}{6144} \pi^2 \right) \left(-\frac{1}{\epsilon} - 8 \ln \frac{\bar{\mu}}{2m(\bar{\mu})} \right) - \right. \\
&\quad - \frac{85291}{768} + \frac{1259}{32} \ln 2 - \frac{5653}{1536} \pi^2 + \frac{1}{4} \gamma_1 - \frac{5}{3} \gamma_2 + \frac{19}{6} \gamma_3 + \\
&\quad \left. + \frac{157}{192} \gamma_4 + \frac{13}{64} (\gamma_5 + \gamma_6) + \frac{4}{9} \gamma_7 + \frac{19}{48} \gamma_8 + \frac{1}{6} \gamma_9 - \gamma_{10} + \mathcal{O}(\epsilon) \right], \tag{6.8}
\end{aligned}$$

$$\tilde{f}_{4,1} = d_A C_A^2 \left[\left(\frac{5}{8} - \frac{5}{64} \pi^2 \right) \left(-\frac{1}{\epsilon} - 8 \ln \frac{\bar{\mu}}{2m(\bar{\mu})} \right) + \right.$$

$$\begin{aligned}
& + \frac{5}{2} + \frac{15}{2} \ln 2 - \frac{115}{192} \pi^2 + \frac{5}{4} (\gamma_4 + \gamma_5) + \mathcal{O}(\epsilon) \Big] + \\
& + d_A C_A^2 (d_A + 2) \left(-\frac{1}{16\epsilon^2} + \ln^2 \frac{\bar{\mu}}{2m(\bar{\mu})} + \frac{1}{2} \ln \frac{\bar{\mu}}{2m(\bar{\mu})} - \right. \\
& \quad \left. - \frac{43}{24} + \frac{11}{12} \ln 2 - \frac{1}{12} \pi^2 + \mathcal{O}(\epsilon) \right), \tag{6.9}
\end{aligned}$$

$$\begin{aligned}
\tilde{f}_{4,2} &= d_A C_A (d_A + 2) \left[\frac{1}{16\epsilon^2} - \frac{32 - \pi^2}{64\epsilon} - \ln^2 \frac{\bar{\mu}}{2m(\bar{\mu})} - \left(\frac{36 - \pi^2}{8} \right) \ln \frac{\bar{\mu}}{2m(\bar{\mu})} - \right. \\
& \quad \left. - \frac{183}{4} + \frac{51}{2} \ln 2 - \frac{23}{48} \pi^2 + 2\gamma_3 + \frac{1}{2} \gamma_4 + \frac{1}{4} \gamma_8 + \mathcal{O}(\epsilon) \right] + \\
& + d_A C_A (d_A + 2)^2 \left(\frac{1}{2} \ln \frac{\bar{\mu}}{2m(\bar{\mu})} - \frac{1}{8} + \mathcal{O}(\epsilon) \right), \tag{6.10}
\end{aligned}$$

$$\begin{aligned}
\tilde{f}_{4,3} &= d_A (d_A + 2) (d_A + 8) \left[\left(\frac{\pi^2}{192} \right) \left(\frac{1}{\epsilon} + 8 \ln \frac{\bar{\mu}}{2m(\bar{\mu})} \right) + \frac{1}{6} \gamma_4 + \mathcal{O}(\epsilon) \right] + \\
& + d_A (d_A + 2)^2 \left(-\frac{1}{2} \ln \frac{\bar{\mu}}{2m(\bar{\mu})} - \frac{1}{4} + \frac{1}{2} \ln 2 + \mathcal{O}(\epsilon) \right) + \\
& + d_A (d_A + 2)^3 \left(\frac{1}{24} + \mathcal{O}(\epsilon) \right). \tag{6.11}
\end{aligned}$$

In particular, following the notation of ref. [11] and writing

$$\tilde{f}_{4,0} \equiv -d_A C_A^3 \left[\alpha_M \left(\frac{1}{\epsilon} + 8 \ln \frac{\bar{\mu}}{2m(\bar{\mu})} \right) + \beta_M \right], \tag{6.12}$$

we read from Eq. (6.8) that

$$\begin{aligned}
\alpha_M &= \frac{43}{32} - \frac{491}{6144} \pi^2 \approx 0.555017, \tag{6.13} \\
\beta_M &= \frac{85291}{768} - \frac{1259}{32} \ln 2 + \frac{5653}{1536} \pi^2 - \frac{1}{4} \gamma_1 + \frac{5}{3} \gamma_2 - \frac{19}{6} \gamma_3 - \\
& \quad - \frac{157}{192} \gamma_4 - \frac{13}{64} (\gamma_5 + \gamma_6) - \frac{4}{9} \gamma_7 - \frac{19}{48} \gamma_8 - \frac{1}{6} \gamma_9 + \gamma_{10} \\
& = -\frac{311}{256} - \frac{43}{32} \ln 2 - \frac{19}{6} \ln^2 2 + \frac{77}{9216} \pi^2 - \frac{491}{1536} \pi^2 \ln 2 + \frac{1793}{512} \zeta(3) + \gamma_{10} \\
& \approx -1.391512. \tag{6.14}
\end{aligned}$$

In Eq. (6.14) we used values for $\gamma_1, \dots, \gamma_{10}$ from Appendix A.5 and Appendix A.6. The coefficient α_M gives a contribution of order $\mathcal{O}(g^6 \ln(1/g) T^4)$ and β_M a perturbative contribution of order $\mathcal{O}(g^6 T^4)$ to the pressure of hot QCD [11].

The expression in Eq. (6.1), with the coefficients in Eqs. (6.2)–(6.11), contains a number of $1/\epsilon^2$ and $1/\epsilon$ -poles. Once our computation is embedded into some physical setting, such as in [11], a vacuum counterterm is automatically generated (denoted by $p_E(T)$ in [11]), which eventually cancels all the UV-poles, such that physical observables remain finite for $\epsilon \rightarrow 0$. The nature of the poles in Eqs. (6.2)–(6.11) is analysed in detail in the next section.

7. Infrared insensitivity of the results

The result shown in the previous section contains a number of $1/\epsilon^2$ and $1/\epsilon$ -divergences. Since dimensional regularisation regulates at the same time both ultraviolet (UV) and infrared (IR) divergences, we may ask of what type are those obtained? The purpose of this section is to show that the divergences are of purely UV origin, and the result is thus IR insensitive, *if interpreted properly*. There are two ways of showing this, firstly an effective theory approach in which one understands that all the IR divergences are contained in the $SU(N_c)$ pure Yang-Mills theory obtained by integrating out the A_0 -field, secondly a pragmatic one in which one shields away the IR divergences by giving the gluon and ghost fields a mass.

Conceptually the best way to analyse the IR sensitivity is to dress the problem in an effective theory language. In the present context, such an analysis was carried out in [10]. The idea is that since the field A_0 has a mass scale, it can be integrated out. The integration out is an ultraviolet procedure, thus by construction not sensitive to IR physics. The effective low-energy theory that emerges is a 3d pure gauge theory. Its partition function, on the other hand, does contain IR divergences, starting at 4-loop level [8, 9].

Therefore, we expect that all results up to 3-loop level should be IR insensitive. At 4-loop level there is a part of the result, that is the diagrams which can be constructed fully inside the pure $SU(N_c)$ theory, which can be both IR and UV divergent. Since in dimensional regularisation, however, these graphs are set to zero, the non-zero result we have obtained should again be insensitive to any mass scales in the gluon and ghost propagators.

Apart from the issue mentioned, there is also another possible source of IR problems, namely that of overlapping divergences. Indeed, while IR divergences appear for vacuum graphs at 4-loop level only, they appear for self-energy graphs already at the 2-loop level (see, e.g., [10]). However, 2-loop self-energy insertions do appear also as subgraphs in the 4-loop “ring diagrams”, making the divergence structure of such 4-loop graphs “doubly” problematic. We return to this issue presently, but first finish the discussion of IR divergences at lower than 4-loop level.

To be very explicit, let us introduce a fictitious mass parameter m_G for all massless lines (gluons and ghosts), hence giving the function $f(m^2, g^2, \lambda)$ a further functional dependence on the mass ratio $x = m_G/m$. Let us denote by AH (“Adjoint Higgs”) graphs with at least one A_0 -line, and by YM (“Yang-Mills”) graphs with none at all. The general structure of the bare $f(m^2, g^2, \lambda)$ can then be expressed as (cf. Eq. (4.14))

$$f(m^2, g^2, \lambda) = \sum_{\ell=1}^{\infty} \left(\frac{\mu^{-2\epsilon}}{4\pi} \right)^\ell \left(\frac{\bar{\mu}}{2m} \right)^{2\epsilon\ell} (g^2)^{\ell-1} m^{4-\ell} \left[\tilde{f}_\ell^{\text{AH}}(x, \epsilon, \xi, \bar{\lambda}) + x^{4-\ell-2\epsilon\ell} \tilde{f}_\ell^{\text{YM}}(\epsilon, \xi) \right], \quad (7.1)$$

where $\tilde{f}_\ell^{\text{AH}}, \tilde{f}_\ell^{\text{YM}}$ are dimensionless functions. While the treatment above corresponds to setting $x = 0$ first and then computing the expansion in ϵ , we now keep a non-zero x through the entire calculation, being interested in the limit of small x only in the end:

$$\overline{\text{MS}} : \quad \lim_{\epsilon \rightarrow 0} \lim_{x \rightarrow 0} \tilde{f}_\ell^{\text{AH}}(x, \epsilon, \xi, \bar{\lambda}), \quad (7.2)$$

$$\text{IR-regulator : } \quad \lim_{x \rightarrow 0} \lim_{\epsilon \rightarrow 0} \tilde{f}_\ell^{\text{AH}}(x, \epsilon, \xi, \bar{\lambda}) . \quad (7.3)$$

These two limits do not in general commute for single diagrams, but should commute for the sum. Possible power IR divergences in single diagrams would show up as poles in x , while logarithmic ones correspond to $\ln x$.

The main technical differences in the IR regularised procedure with respect to the $\overline{\text{MS}}$ computation are a more complicated scalarisation, in the absence of low-level routines specific to the presence of massless lines, such as the so-called “triangle rule”, and an enlarged set of master integrals. Furthermore, some additional diagrams contribute, which were set to zero from the outset in the $\overline{\text{MS}}$ calculation, due to the absence of any mass scale (in some subdiagram).

As a roundup, it turns out that, starting at the 3-loop level, individual diagrams *do* indeed contain logarithmic as well as powerlike IR divergences, which then cancel in the sum, proving *a posteriori* the validity of the dimensionally regularised $\overline{\text{MS}}$ calculation. For completeness, we illustrate this issue in Appendix B.

We now return to the 4-loop level. According to the discussion above, the full set of graphs can be divided into four sub-classes, having potentially different IR properties: pure Yang–Mills graphs (YM) and those with at least one A_0 -line (AH), with both sets further divided into skeletons (Fig. 1) and ring diagrams (Fig. 2). The properties of the pure Yang–Mills diagrams are discussed in [12], and we only state here that they contain both logarithmic UV as well as IR divergences, which however exactly cancel in strict dimensional regularisation (but not in regularisations which only regulate the UV, such as lattice regularisation). Here we then just discuss the skeletons and rings containing at least one massive A_0 -line. For simplicity, we discuss explicitly only terms without a quartic coupling λ .

We have computed the $1/\epsilon$ -divergence in the sum of such AH-skeletons with in total three different mass spectra:

1. As described above, whereby the A_0 -lines carry the mass parameter m^2 , while the gluon and ghost lines are massless.
2. By giving an equal mass to all the fields: A_0 , gluons, and ghosts. The computation proceeds in complete analogy with the one described in [12].
3. By setting all masses to zero, picking some line in the 4-loop vacuum graph, integrating the massless 3-loop 2-point function connected to that line in d dimensions⁵, and regulating the remaining single integral by shielding the IR with a mass and regulating the UV via dimensional regularization.

All three methods give the same result for the $1/\epsilon$ -pole in AH-skeletons, confirming its expected IR finiteness. Expressed as a contribution to \tilde{p}_4 in Eq. (4.18), the divergence appearing

⁵This problem has been solved a long time ago via integration by parts; for a discussion as well as an algorithmic implementation, see [23].

in the result reads

$$\delta[\tilde{p}_4] = \frac{1}{3072\epsilon} \left[3(696 - 56\xi - 6\xi^2 - 5\xi^3) - \frac{\pi^2}{4}(832 - 144\xi + 81\xi^2 - 15\xi^3 + 3\xi^4) \right]. \quad (7.4)$$

For the AH-rings, on the other hand, the third method does not work. This is due to the overlapping divergences mentioned above: a 2-loop 2-point function of gluons alone leads to logarithmic UV and IR divergences, and trying to carry out the final integration by some recipe, gives generically an outcome $\sim 1/\epsilon^2$, but with a coefficient dependent on what the recipe precisely was. To cancel the $1/\epsilon^2$ -pole, not to mention to get the correct coefficient for the remaining $1/\epsilon$ -pole, is a very delicate problem, which can only be guaranteed to have been solved by employing a fully systematic procedure. Our non-Abelian case is therefore qualitatively different from a pure scalar theory, where the problem of overlapping divergences does not emerge [24]. For a discussion of the cancellation of the analogue of the $1/\epsilon^2$ -pole in cutoff regularisation in the pure $SU(N_c)$ theory, see [15].

On the contrary, the AH-rings can be systematically computed with the 1st and 2nd types of mass spectra. Both procedures give the same result, confirming its IR insensitivity. Summing together with Eq. (7.4), we recover the ξ -independent $1/\epsilon$ -pole on the first row in Eq. (4.18).

In summary, we have verified explicitly that the only possible IR divergence appearing in our computation is that of the pure $SU(N_c)$ gauge theory, contained in the YM-graphs. It is addressed further in ref. [12].

8. Discussion and conclusions

The main point of this paper has been the discussion of formal analytic techniques for, and actual results from, the evaluation of the 4-loop partition function of the 3d $SU(N_c) + \text{adjoint Higgs}$ theory using dimensional regularisation. The final result is shown in Eqs. (6.1)–(6.11). We have also demonstrated that if interpreted as a matching coefficient — that is, if the pure Yang-Mills graphs, without any adjoint scalar lines, are dropped, as is automatically the case in strict dimensional regularisation — then the result is IR finite. Therefore, all IR divergences are contained in the pure Yang-Mills theory. We would now like to end by recalling that such techniques and results have also practical applications.

Perhaps the most important application is that our results provide two specific new *perturbative* contributions to the free energy of hot QCD, of orders $g^6 \ln(1/g)T^4$, $g^6 T^4$ [11]. Similarly, they provide also new perturbative contributions to quark number susceptibilities [25]. Once the parameters of the 3d theory are expressed in terms of the parameters of the physical finite temperature QCD via dimensional reduction, and once other contributions of the same parametric magnitudes are added, this allows for instance to re-estimate the convergence properties of QCD perturbation theory at high temperatures [11, 25, 26]. Our present computation also contributes to the $\overline{\text{MS}}$ scheme renormalisation of the simplest 3d gauge-invariant local condensates, obtained by partial derivatives of the action with respect

to various parameters [21], and thus in principle helps in non-perturbative studies of the pressure of high-temperature QCD [4, 13]. It may also allow for refined analytic estimates such as Padé resummations [27] for the observable in Eq. (1.3).

Let us mention that there has recently been significant interest in somewhat more phenomenological approaches to QCD perturbation theory at high temperatures (for reviews see, e.g., [28]). As far as we can tell our results are of no immediate use in such settings.

Another application is that our general procedure is relevant for studies of critical phenomena in some statistical physics systems. In this context one may either study directly the three-dimensional physical system, or carry out computations first in $d = 4 - \epsilon$ dimensions, expand in ϵ , and then take the limit $\epsilon \rightarrow 1$. For instance, some properties of the Ginzburg–Landau theory of superconductivity have been addressed in the former setup up to 2-loop level (see, e.g., [29]–[32]), and in the latter setup, in the disordered phase, up to 3-loop level [33]. The integrals arising in the disordered phase are “QED-like” just as in our study, so that scalarisation and the sets of master integrals are essentially the same as the present ones [16]. Moreover, in the case $d = 4 - \epsilon$, the master integrals can be evaluated to a high accuracy utilising the techniques introduced in [34], while for $d = 3 - 2\epsilon$ most master integrals have been evaluated in this paper. Our methods could therefore help in reaching the 4-loop order.

Acknowledgements

We are indebted to J.A.M. Vermaseren for discussions as well as for his continuing efforts in optimising FORM, and to A. Rajantie and A. Vuorinen for discussions. This work was partly supported by the RTN network *Supersymmetry and the Early Universe*, EU contract no. HPRN-CT-2000-00152, and by the Academy of Finland, contracts no. 77744 and 80170.

Appendix A. Master integrals

We discuss in this Appendix the determination of the scalar master integrals of Eqs. (4.3)–(4.13). They depend on one mass-scale m only and are thus “QED-like” in the generalised sense that the number of massive lines at each vertex is even. Since the dependence on m is trivial and has been absorbed into the coefficients, see Eq. (4.2), $m = 1$ in most of what follows. One obtains particularly simple expansions in $3 - 2\epsilon$ dimensions by using the integration measure $\int_p = \frac{(4\pi e^\gamma)^\epsilon}{2\pi^2} \int d^{3-2\epsilon} p$, in accordance with Eq. (4.2).

We first discuss briefly the various general techniques we have employed for the evaluation of these integrals. The list of techniques includes: partial integration relations between various scalar integrals, in analogy with those derived at 3-loop level in [20] (Appendix A.1); graphs with only two massive lines, which can often be evaluated exactly (Appendix A.2); graphs with two or three vertices, which can be evaluated to a sufficient depth in ϵ using con-

figuration space methods (Appendix A.3); and some remaining graphs, which were evaluated in momentum space (Appendix A.4). We combine the results from the various techniques in Appendix A.5, showing the actual expansions for the master integrals to the depths specified in Eqs. (4.3)–(4.11). There is one finite integral remaining which we have not been able to evaluate analytically, corresponding to Eq. (4.12); its numerical value is determined in Appendix A.6.

A.1. Partial integration identities

Implementing systematically all identities following from partial integrations, as discussed in Sec. 3, allows not only to express all integrals in terms of a few scalar ones, which do not contain any non-trivial numerators, but produces also a set of relations between the scalar integrals. As a simple example, we may recall that the identity

$$0 = \sum_{k=1}^d \int_{p,q} \frac{\partial}{\partial p_k} \left[\frac{p_k - q_k}{(p^2 + m^2)(q^2 + m^2)(p - q)^2} \right], \quad (\text{A.1})$$

leads to the relation

$$\int_{p,q} \frac{1}{(p^2 + m^2)(q^2 + m^2)(p - q)^2} = \frac{1}{d - 3} \int_p \frac{1}{(p^2 + m^2)^2} \int_q \frac{1}{(q^2 + m^2)}. \quad (\text{A.2})$$

Taking furthermore into account that in dimensional regularisation the two integrals on the right-hand-side of Eq. (A.2) are related, we obtain

$$\textcircled{\dots} = \frac{1}{m^2} \left(\textcircled{} \right)^2 \left[-\frac{(d-2)}{2(d-3)} \right]. \quad (\text{A.3})$$

Examples of similar relations at 3-loop level were shown in Eqs. (3.1), (3.2), and a complete 3-loop analysis can be found in [20] (see also [6]).

At 4-loop level, there are obviously many more identities than at 3-loop level. Rather than showing a complete list we give here, as an example, one of the relations:

$$\textcircled{\diagup} = \frac{1}{m^2} \textcircled{} \times \textcircled{\textcircled{}} \left[-\frac{d-2}{2(d-3)} \right] + \frac{1}{m^2} \textcircled{\textcircled{\diagup}} \left[\frac{2d-5}{4(d-3)} \right]. \quad (\text{A.4})$$

It turns out that this relation is convenient for the determination of the 4-loop integral on the right-hand-side.

A.2. Integrals known exactly

A few of the integrals appearing can be evaluated exactly in d dimensions. This holds particularly for cases where only two massive propagators appear. As an example, we show how this can be done in configuration space. The massive propagator can be written as

$$G(x; m_i) \equiv \int \frac{d^{3-2\epsilon} p}{(2\pi)^{3-2\epsilon}} \frac{e^{ip \cdot x}}{p^2 + m_i^2} = \frac{1}{(2\pi)^{\frac{3}{2}-\epsilon}} \left(\frac{m_i}{x} \right)^{\frac{1}{2}-\epsilon} K_{\frac{1}{2}-\epsilon}(m_i x), \quad (\text{A.5})$$

where K is a modified Bessel function, and x denotes, depending on the context, either a d -dimensional vector or its modulus. On the other hand, the massless part of the graph converts in configuration space to

$$\int \frac{d^{3-2\epsilon} p}{(2\pi)^{3-2\epsilon}} \frac{e^{ip \cdot x}}{p^\nu} = \frac{\Gamma(\frac{3}{2} - \frac{\nu}{2} - \epsilon)}{\Gamma(\frac{\nu}{2})} \frac{1}{2^\nu \pi^{\frac{3}{2} - \epsilon} x^{3-\nu-2\epsilon}}. \quad (\text{A.6})$$

We can then employ the identity

$$\int_0^\infty dx x^\lambda K_\mu^2(x) = \frac{2^{\lambda-2}}{\Gamma(1+\lambda)} \Gamma\left(\frac{1+\lambda+2\mu}{2}\right) \Gamma^2\left(\frac{1+\lambda}{2}\right) \Gamma\left(\frac{1+\lambda-2\mu}{2}\right). \quad (\text{A.7})$$

With this result, the following expressions are easily derived (using the integration measure inside the curly brackets in Eq. (4.2)):

$$\text{Diagram 1} = \left(-\frac{1}{2\epsilon}\right) \frac{(4e^\gamma)^{3\epsilon} \Gamma(\frac{1}{2} + \epsilon) \Gamma(\frac{1}{2} - \epsilon) \Gamma(\frac{1}{2} + 3\epsilon) \Gamma^2(1 + 2\epsilon)}{(1 - 2\epsilon)(1 - 6\epsilon) \Gamma^3(\frac{1}{2}) \Gamma(1 + 4\epsilon)} \quad (\text{A.8})$$

$$= -\frac{1}{2\epsilon} - 4 - \left(26 + \frac{25}{24} \pi^2\right) \epsilon - \left(160 + \frac{25}{3} \pi^2 - \frac{47}{2} \zeta(3)\right) \epsilon^2 + \mathcal{O}(\epsilon^3), \quad (\text{A.9})$$

$$\text{Diagram 2} = \frac{\pi^2}{32\epsilon} (4e^\gamma)^{4\epsilon} \frac{\Gamma^2(\frac{1}{2} + \epsilon) \Gamma^3(\frac{1}{2} - \epsilon) \Gamma^2(\frac{1}{2} + 3\epsilon) \Gamma(\frac{1}{2} - 3\epsilon) \Gamma(1 + 4\epsilon)}{(1 - 2\epsilon) \Gamma^8(\frac{1}{2}) \Gamma^2(1 - 2\epsilon) \Gamma(1 + 6\epsilon)} \quad (\text{A.10})$$

$$= \frac{\pi^2}{32} \left[\frac{1}{\epsilon} + 2 + 4 \ln 2 + \left(4 + \frac{17}{3} \pi^2 + 8 \ln 2 (1 + \ln 2)\right) \epsilon + \mathcal{O}(\epsilon^2) \right], \quad (\text{A.11})$$

$$\text{Diagram 3} = \frac{3}{8\epsilon} (4e^\gamma)^{4\epsilon} \frac{\Gamma^2(\frac{1}{2} - \epsilon) \Gamma^2(\frac{1}{2} + 3\epsilon) \Gamma(1 + 2\epsilon) \Gamma(1 + 4\epsilon)}{(1 - 2\epsilon)(1 - 4\epsilon)(1 - 6\epsilon) \Gamma^4(\frac{1}{2}) \Gamma(1 + 6\epsilon)} \quad (\text{A.12})$$

$$= \frac{3}{8\epsilon} + \frac{9}{2} + \left(\frac{75}{2} + \frac{11}{8} \pi^2\right) \epsilon + \left(270 + \frac{33}{2} \pi^2 - \frac{55}{2} \zeta(3)\right) \epsilon^2 + \mathcal{O}(\epsilon^3). \quad (\text{A.13})$$

Obviously we also know (f_p is again according to the curly brackets in Eq. (4.2)):

$$\text{Diagram 4} = \int_p \frac{1}{p^2 + 1} = -\frac{(4e^\gamma)^\epsilon}{1 - 2\epsilon} \frac{\Gamma(\frac{1}{2} + \epsilon)}{\Gamma(\frac{1}{2})} \quad (\text{A.14})$$

$$= -1 - 2\epsilon - \left(4 + \frac{\pi^2}{4}\right) \epsilon^2 - \left(8 + \frac{\pi^2}{2} - \frac{7}{3} \zeta(3)\right) \epsilon^3 + \mathcal{O}(\epsilon^4). \quad (\text{A.15})$$

A.3. Configuration space evaluations

Even when configuration space does not allow for an exact evaluation of the integral, like in Appendix A.2, it may allow for the most straightforward way of obtaining a number of coefficients in an expansion of the result in ϵ . This is the case particularly if there are only two vertices in the graph.

At ℓ -loop level, the graphs in this class are of the form

$$1 \left(2 \left(\dots \right) \right)^{\ell+1} = \left[4\pi \left(\frac{e^\gamma}{\pi} \right)^\epsilon \right]^\ell \frac{2\pi^{\frac{3}{2} - \epsilon}}{\Gamma(\frac{3}{2} - \epsilon)} \int_0^\infty dx x^{2-2\epsilon} \prod_{i=1}^{\ell+1} G(x; m_i), \quad (\text{A.16})$$

where $G(x; m_i)$ is from Eq. (A.5). The idea (see, e.g., [24]) is to split the integration into two parts: $\int_0^\infty dx(\dots) = \int_0^r dx(\dots) + \int_r^\infty dx(\dots)$. The first part is performed in $d = 3 - 2\epsilon$ dimensions but by using the asymptotic small- x form of $G(x; m_i)$,

$$G(x; m_i) = \frac{\Gamma(\frac{1}{2} - \epsilon)}{4\pi^{\frac{3}{2} - \epsilon}} \frac{1}{x^{1-2\epsilon}} \left[1 - \left(\frac{m_i x}{2}\right)^{1-2\epsilon} \frac{\Gamma(\frac{1}{2} + \epsilon)}{\Gamma(\frac{3}{2} - \epsilon)} + \left(\frac{m_i x}{2}\right)^2 \frac{\Gamma(\frac{1}{2} + \epsilon)}{\Gamma(\frac{3}{2} + \epsilon)} + \dots \right], \quad (\text{A.17})$$

while the latter part, which is finite, is performed by expanding first in ϵ and then carrying out the remaining integrals in $d = 3$ dimensions. For instance,

$$G(x; m_i) = \frac{e^{-m_i x}}{4\pi x} \left[1 - \epsilon \left(\ln \frac{m_i^2 e^\gamma}{4\pi} + m_i x \int_1^\infty dy \ln(y^2 - 1) e^{(1-y)m_i x} \right) + \mathcal{O}(\epsilon^2) \right]. \quad (\text{A.18})$$

When the two parts are summed together and the limit $r \rightarrow 0$ is taken, the dependence on r cancels, and we obtain the desired result.

In the evaluation of such integrals, dilogarithms will in general appear. Their properties have been summarised, e.g., in [35]. For completeness, let us recall here that one can shift the argument of

$$\text{Li}_2(x) = - \int_0^x dt \frac{\ln(1-t)}{t} = \sum_{n>0} \frac{x^n}{n^2} \quad (\text{A.19})$$

from the intervals $[-\infty\dots-1]$, $[-1\dots0]$, $[1/2\dots1]$ to the interval $[0\dots1/2]$ via

$$\text{Li}_2(x) = \text{Li}_2\left(\frac{1}{1-x}\right) - \ln(1-x) \ln(-x) + \frac{1}{2} \ln^2(1-x) - \frac{\pi^2}{6}, \quad (\text{A.20})$$

$$\text{Li}_2(x) = -\text{Li}_2\left(-\frac{x}{1-x}\right) - \frac{1}{2} \ln^2(1-x), \quad (\text{A.21})$$

$$\text{Li}_2(x) = -\text{Li}_2(1-x) - \ln(1-x) \ln x + \frac{\pi^2}{6}, \quad (\text{A.22})$$

respectively. As follows from here, the dilogarithms satisfy, for $x > 0$,

$$\text{Li}_2(-x) + \text{Li}_2\left(-\frac{1}{x}\right) = -\frac{1}{2} \ln^2 x - \frac{\pi^2}{6}. \quad (\text{A.23})$$

Special values include

$$\text{Li}_2(-1) = -\frac{\pi^2}{12}, \quad \text{Li}_2(0) = 0, \quad \text{Li}_2\left(\frac{1}{2}\right) = \frac{\pi^2}{12} - \frac{1}{2} \ln^2 2, \quad \text{Li}_2(1) = \frac{\pi^2}{6}. \quad (\text{A.24})$$

Using these identities, and denoting $M = m_1 + m_2 + m_3$, we obtain for the 2-loop case

$$\frac{1}{\left(\frac{2}{3}\right)} = \left(\frac{2}{M}\right)^{4\epsilon} \left\{ \frac{1}{4\epsilon} + \frac{1}{2} + \epsilon \left[1 - \frac{\pi^2}{24} + \sum_{i=1}^3 \text{Li}_2\left(1 - \frac{2m_i}{M}\right) \right] + \mathcal{O}(\epsilon^2) \right\}. \quad (\text{A.25})$$

For the 3-loop case, now denoting $M = m_1 + m_2 + m_3 + m_4$, we obtain

$$\begin{aligned}
1 \text{ (two overlapping circles)} 4 = & -M \left(\frac{2}{M} \right)^{6\epsilon} \left\{ \frac{1}{4\epsilon} + 2 + \frac{1}{2} \sum_{i=1}^4 \frac{m_i}{M} \ln \frac{M}{2m_i} \right. \\
& + \epsilon \left[13 + \frac{3}{16} \pi^2 + \sum_{i=1}^4 \left(\left(1 - \frac{2m_i}{M} \right) \text{Li}_2 \left(1 - \frac{2m_i}{M} \right) \right. \right. \\
& \left. \left. + 4 \frac{m_i}{M} \ln \frac{M}{2m_i} + \frac{1}{2} \frac{m_i}{M} \ln^2 \frac{M}{2m_i} \right) \right] + \mathcal{O}(\epsilon^2) \left. \right\}. \quad (\text{A.26})
\end{aligned}$$

In particular, if all masses are equal,

$$\text{two overlapping circles} = -\frac{1}{\epsilon} - 8 + 4 \ln 2 - 4\epsilon \left(13 + \frac{17}{48} \pi^2 - 8 \ln 2 + \ln^2 2 \right) + \mathcal{O}(\epsilon^2). \quad (\text{A.27})$$

The case of two massless and two massive lines can be checked against Eq. (A.9).

The 4-loop case has only been worked out to order $\mathcal{O}(1)$, rather than $\mathcal{O}(\epsilon)$. Denoting now $M = m_1 + m_2 + m_3 + m_4 + m_5$,

$$1 \text{ (four overlapping circles)} 5 = M^2 \left(\frac{2}{M} \right)^{8\epsilon} \left[\frac{1}{16\epsilon} + \frac{3}{4} + \sum_{i \neq j} \frac{m_i m_j}{2M^2} \left(\frac{1}{8\epsilon} + \frac{3}{2} + \ln \frac{M}{2m_i} \right) + \mathcal{O}(\epsilon) \right]. \quad (\text{A.28})$$

The case of three massless and two massive lines can be checked against Eq. (A.13). The next order, $\mathcal{O}(\epsilon)$, could also be worked out and is indeed needed for γ_8 in Eq. (4.10), but we choose to use another way to determine it, based on Eq. (A.4).

When there are more than two vertices in the graph, the configuration space technique gets rapidly more complicated, due to the difficult structure of the angular integrals. There is one graph we are interested in, however, whose divergent and, most incredibly, also the constant part [36] can still be obtained analytically:

$$2 \text{ (a circle with a vertical line and a diagonal line)} 6 = \left[4\pi \left(\frac{e^\gamma}{\pi} \right)^\epsilon \right]^4 \int d^{3-2\epsilon} x \int d^{3-2\epsilon} y G(x-y; m_1) \prod_{i=2}^3 G(x; m_i) \prod_{j=4}^6 G(y; m_j). \quad (\text{A.29})$$

Employing the angular integral [37]

$$\int d\Omega_y \frac{K_\lambda(|x-y|)}{|x-y|^\lambda} = \frac{(2\pi)^{\lambda+1}}{(xy)^\lambda} \left[\theta(x-y) K_\lambda(x) I_\lambda(y) + \theta(y-x) K_\lambda(y) I_\lambda(x) \right], \quad (\text{A.30})$$

where $\lambda = \frac{1}{2} - \epsilon$ and on the right-hand-side $x \equiv |x|$, $y \equiv |y|$, one is left with two independent radial integrations which can be handled as above [36], by splitting the integrations as $\int_0^\infty dx(\dots) = \int_0^r dx(\dots) + \int_r^\infty dx(\dots)$. Denoting $M_{123} = m_1 + m_2 + m_3$, $M_{23456} = m_2 + m_3 + m_4 + m_5 + m_6$, the outcome is

$$2 \text{ (a circle with a vertical line and a diagonal line)} 6 = \left(\frac{2}{M_{123}} \right)^{8\epsilon} \frac{1}{32} \left[\frac{1}{\epsilon^2} + \frac{8}{\epsilon} + 4\phi \left(\frac{M_{123}}{M_{23456}}, \frac{2m_2}{M_{123}}, \frac{2m_1}{M_{123}} - 1 \right) + \mathcal{O}(\epsilon) \right], \quad (\text{A.31})$$

where

$$\begin{aligned}
\phi(x, y, z) &= 13 + \frac{7}{12} \pi^2 - 4 \ln^2 x + \\
&+ 2\text{Li}_2(1-y) + 2\text{Li}_2(y+z) + 2\text{Li}_2(-z) + 8 \frac{1-x}{x(1+z)} \text{Li}_2(1-x) + \\
&+ 8 \left(1 + \frac{1-x}{x(1+z)} \right) \left(\text{Li}_2(-xz) + \ln x \ln(1+xz) - \frac{\pi^2}{6} \right). \tag{A.32}
\end{aligned}$$

In particular,

$$\textcircled{V} = \frac{1}{32} \left[\frac{1}{\epsilon^2} + \frac{8}{\epsilon} + 4 \left(13 - 8 \ln^2 2 - \frac{13}{12} \pi^2 \right) + \mathcal{O}(\epsilon) \right]. \tag{A.33}$$

A.4. Momentum space evaluations

When the graph has more than two vertices, the configuration space method is in general no longer practical. Some of these graphs are, however, rather easily evaluated in momentum space. This is the case particularly for the ‘‘triangle’’ topology, shown in Eq. (A.38) below.

The triangle graph consists of three consecutive 1-loop self-energy insertions,

$$\int \frac{d^{3-2\epsilon} q}{(2\pi)^{3-2\epsilon}} \frac{1}{[q^2 + m_1^2][(q+p)^2 + m_2^2]} = \frac{\Gamma(\frac{1}{2} + \epsilon)}{(4\pi)^{\frac{3}{2} - \epsilon} p^{1+2\epsilon}} B(p, m_1, m_2, \epsilon), \tag{A.34}$$

where $B(p, m_1, m_2, \epsilon)$ is a one-dimensional integral over a Feynman parameter. It has the properties

$$B(0, m_1, m_2, \epsilon) = 0, \tag{A.35}$$

$$B(p, 0, 0, \epsilon) = \lim_{p \rightarrow \infty} B(p, m_1, m_2, \epsilon) = \frac{\Gamma^2(\frac{1}{2} - \epsilon)}{\Gamma(1 - 2\epsilon)}, \tag{A.36}$$

$$B(p, m_1, m_2, 0) = 2 \arctan \frac{p}{m_1 + m_2}. \tag{A.37}$$

The triangle graph is then just a one-dimensional integration over the modulus of p . Carrying out one partial integration and expanding in ϵ , one obtains [36]

$$\textcircled{1} = \left(\frac{2}{m_1 + m_2} \right)^{8\epsilon} \frac{\pi^2}{32} \left[\frac{1}{\epsilon} + 2 + 4 \ln 2 - \chi \left(\frac{m_3 + m_4}{m_1 + m_2}, \frac{m_5 + m_6}{m_1 + m_2} \right) + \mathcal{O}(\epsilon) \right], \tag{A.38}$$

where

$$\chi(x, y) = \frac{64}{\pi^3} \int_0^\infty dp \ln p \frac{d}{dp} \left[\arctan(p) \arctan \left(\frac{p}{x} \right) \arctan \left(\frac{p}{y} \right) \right], \tag{A.39}$$

$$\chi(1, 1) = \frac{84}{\pi^2} \zeta(3), \quad \chi(1, 0) = \frac{56}{\pi^2} \zeta(3), \quad \chi(0, 0) = 0. \tag{A.40}$$

A.5. Summary of expansions for master integrals

Given the results of the previous sections, we can collect together the expressions for the constants $\gamma_1, \dots, \gamma_9$ defined in Eqs. (4.3)–(4.11). From Eq. (A.15),

$$\gamma_1 = -8 - \frac{\pi^2}{2} + \frac{7}{3} \zeta(3). \quad (\text{A.41})$$

Combining Eq. (3.1) with Eq. (A.9),

$$\gamma_2 = \frac{1}{6} \pi^2 - \frac{5}{2} \zeta(3). \quad (\text{A.42})$$

Combining Eq. (3.2) with Eq. (A.27),

$$\gamma_3 = -\frac{1}{6} \pi^2 - \ln^2 2. \quad (\text{A.43})$$

From Eqs. (A.38), (A.40) (or, for γ_6 , from Eq. (A.11)),

$$\gamma_4 = \frac{\pi^2}{32} \left(2 + 4 \ln 2 - \frac{84}{\pi^2} \zeta(3) \right), \quad (\text{A.44})$$

$$\gamma_5 = \frac{\pi^2}{32} \left(2 + 4 \ln 2 - \frac{56}{\pi^2} \zeta(3) \right), \quad (\text{A.45})$$

$$\gamma_6 = \frac{\pi^2}{32} \left(2 + 4 \ln 2 \right), \quad (\text{A.46})$$

$$\gamma_7 = \frac{\pi^2}{32} \left(2 + 12 \ln 2 - \frac{84}{\pi^2} \zeta(3) \right). \quad (\text{A.47})$$

Combining Eqs. (A.33), (A.4),

$$\gamma_8 = 175 - 96 \ln 2 + 16 \ln^2 2 + \frac{53}{12} \pi^2. \quad (\text{A.48})$$

Finally, from Eq. (A.13),

$$\gamma_9 = 270 + \frac{33}{2} \pi^2 - \frac{55}{2} \zeta(3). \quad (\text{A.49})$$

A.6. Numerical evaluation of γ_{10}

It can easily be verified that the integrals in Eqs. (4.12), (4.13) are both infrared and ultra-violet finite. They can therefore be evaluated directly in $d = 3$ dimensions. For the present application we only need γ_{10} , defined by Eq. (4.12).

There is no obvious partial integration relation whereby γ_{10} could be reduced to a simpler integral. Due to the fact that there are four vertices, it is also not easily treated in configuration space. The most straightforward approach seems then to be to combine the self-energy of Eqs. (A.34), (A.37) with the 2-loop self-energy

$$\text{---} \bigcirc \text{---}, \quad (\text{A.50})$$

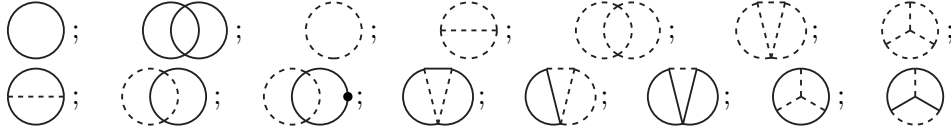


Figure 5: A possible choice for 1-loop, 2-loop and 3-loop “master” topologies, in the case that gluons and ghosts are treated as particles with a mass m_G . There are no numerators left in these graphs. A solid line is a propagator of the form $1/(p^2 + m^2)$, and a dashed line of the form $1/(p^2 + m_G^2)$, where p is the Euclidean momentum flowing through the line. A line with a blob on it indicates a squared propagator, $1/(p^2 + m^2)^2$.

for which a one-dimensional integral representation has been given in [38]. This leads to a simple two-dimensional integral representation:

$$\gamma_{10} = \frac{2}{\pi} \int_0^\infty dp p \arctan \frac{p}{2} \cdot \Pi_2(p), \quad (\text{A.51})$$

where [38]

$$\begin{aligned} \Pi_2(p) = \frac{1}{p^3} \int_{x_-(p)}^1 \frac{dx}{\sqrt{p^2 x^2 - (1-x^2)^2}} & \left\{ \frac{p}{1-x^2} \left[(1+x^2) \arctan \frac{p}{2} - \right. \right. \\ & \left. \left. -2(1-x+x^2) \arctan \frac{p}{1+x} + \frac{\pi}{2}(1-x)^2 \right] + x \ln \left[1 + \frac{p^2}{(1+x)^2} \right] \right\}, \quad (\text{A.52}) \end{aligned}$$

and $x_-(p) \equiv (1+p^2/4)^{\frac{1}{2}} - p/2$. We may note that in Eq. (A.52) it is numerically advantageous to change the integration variable from x to $y \equiv \sqrt{x - x_-(p)}$. The final result reads

$$\gamma_{10} \approx 0.171007009753(1), \quad (\text{A.53})$$

where the number in parentheses indicates the uncertainty in the last digit.

Appendix B. Three-loop results with and without an IR cutoff

As discussed in Sec. 7, starting at the 3-loop level single graphs are considerably more infrared sensitive than the total sum: the limits in Eqs. (7.2), (7.3) commute only for the latter. Let us recall that there $x = m_G/m$, where m_G is a fictitious mass given to the gluons and ghosts:

$$\langle A_k^a(p) A_l^b(-p) \rangle \equiv \frac{\delta^{ab}}{p^2 + m_G^2} \left(\delta_{kl} - p_k p_l \frac{\xi}{p^2 + m_G^2} \right), \quad \langle c^a(p) \bar{c}^b(p) \rangle \equiv \frac{\delta^{ab}}{p^2 + m_G^2}, \quad (\text{B.1})$$

where A_k^a, c^a, \bar{c}^b are the gluon, ghost, and anti-ghost fields, respectively. We illustrate the general structures appearing here with a few specific examples.

In the presence of the two mass scales m, m_G , the set of master integrals is more complicated than when gluons and ghosts are massless. The master integrals that can appear in principle are shown in Fig. 5, up to 3-loop level.

It turns out that the skeleton diagrams are better behaved in the IR than the ring diagrams: power and logarithmic IR divergences appear only in single rings, but they cancel in their sum. A rather typical example, with both an UV pole $1/\epsilon$ and an IR divergence $\ln(m_G/m)$, is given by the gluon ring with a scalar and ghost bubble attached to it. Carrying out scalarisation to the master integrals shown in Fig. 5, denoting $x = m_G/m$, and normalising as in Eq. (3.7), we obtain

$$\begin{aligned}
-\frac{1}{4} \left(\text{Diagram} \right) \Big|_{x \neq 0} &= \frac{1}{m^2} \left(\text{Diagram} \right)^2 \times \left(\text{Diagram} \right) \left[-\frac{(d-2)}{8(d-1)x^2} \right] + \\
&+ \frac{1}{m^2} \left(\text{Diagram} \right) \times \left(\text{Diagram} \right)^2 \left[\frac{(d-2)}{432(d-1)x^2} \right] \times \left(54 + 54d + 18\xi - 18d^2\xi - \right. \\
&\quad \left. - 14\xi^2 + 14d\xi^2 - d^2\xi^2 + d^3\xi^2 \right) + \\
&+ \left(\text{Diagram} \right) \times \left(\text{Diagram} \right) \left[\frac{(20-8d-6x^2+3dx^2)}{16(d-1)x^2} \right] + \\
&+ \left(\text{Diagram} \right) \times \left(\text{Diagram} \right) \left[\frac{1}{1296(d-1)} \right] \times \left(1134 - 459d + 54d^2 + 108\xi - \right. \\
&\quad \left. - 90d\xi - 18d^3\xi - 84\xi^2 + 76d\xi^2 + 5d^2\xi^2 + 2d^3\xi^2 + d^4\xi^2 \right) + \\
&+ \left(\text{Diagram} \right) \left[-\frac{(32-12d-6x^2+3dx^2)}{32(d-1)x^2} \right] + \\
&+ m^2 \left(\text{Diagram} \right) \left[-\frac{(-1+x^2)}{2(d-1)x^2} \right] + \\
&+ m^2 \left(\text{Diagram} \right) \left[-\frac{(44-8d-14x^2+5dx^2)}{32(d-1)} \right]. \tag{B.2}
\end{aligned}$$

According to Eq. (7.3), the first step is now to expand in $\epsilon \ll 1$. The integrals emerging are all known [6, 38]. Changing the normalisation to be according to Eq. (4.17), we obtain

$$\begin{aligned}
\delta \tilde{p}_3 \Big|_{x \neq 0} &= -\frac{1}{32\epsilon} (\xi - 1)^2 + \frac{20 + x^2}{128x} \left[-\text{Li}_2 \left(\frac{3x}{2(1+x)} \right) - \text{Li}_2 \left(-\frac{x}{2+x} \right) - \right. \\
&\quad \left. - \ln \left(1 - \frac{x}{2} \right) \ln \frac{3x}{2(1+x)} - \frac{1}{2} \ln^2(1+x) + \frac{1}{2} \ln \left(1 + \frac{x}{2} \right) \ln \frac{9x^2}{2(2+x)} \right] - \\
&\quad - \frac{4-3x^2}{32x} \ln \left(1 + \frac{x}{2} \right) - \frac{(1+x)(3x-4)}{32x} \ln(1+x) + \frac{3x}{32} + \\
&\quad + \frac{1}{32} (2\xi - 3)(2\xi - 1) \ln \frac{3x}{2} - \frac{837 - 954\xi + 409\xi^2}{2592} + \mathcal{O}(\epsilon). \tag{B.3}
\end{aligned}$$

The second step is then to expand in $x \ll 1$:

$$\delta \tilde{p}_3 \Big|_{\text{Eq. (7.3)}} = -\frac{1}{32\epsilon} (\xi - 1)^2 + \frac{2 - 2\xi + \xi^2}{8} \ln \frac{3x}{2} - \frac{1080 - 954\xi + 409\xi^2}{2592} + \mathcal{O}(x, \epsilon). \tag{B.4}$$

We observe that there is a gauge-parameter dependent UV-divergence in the form of $1/\epsilon$, and a gauge-parameter dependent logarithmic IR divergence in the form of $\ln x$.

Proceeding according to Eq. (7.2), on the other hand, leads to

$$-\frac{1}{4} \left(\text{Diagram: circle with two internal lines and arrows} \right) \Big|_{x=0} = \frac{1}{m^2} \left(\text{Diagram: empty circle} \right)^3 \left[-\frac{(d-2)^2}{16(d-3)(2d-7)(3d-8)} \right] + m^2 \left(\text{Diagram: circle with a vertical line through the center} \right) \left[\frac{(d-3)}{4(2d-7)(3d-8)} \right], \quad (\text{B.5})$$

in terms of the master integrals in Fig. 4. Expanding in $\epsilon \ll 1$,

$$\delta \tilde{p}_3|_{\text{Eq. (7.2)}} = \frac{1}{32\epsilon} + \frac{1}{8} + \mathcal{O}(\epsilon). \quad (\text{B.6})$$

Clearly Eqs. (B.4), (B.6) do not agree⁶. Summing all the graphs together, however, both procedures lead to the gauge-parameter independent and UV and IR finite \tilde{p}_3 on the first row in Eq. (4.17): in other words, ξ , $1/\epsilon$ and $\ln x$ all cancel.

Some other rings lead also to $1/x$ -divergences. Let us show, as an example,

$$\frac{1}{16} \left(\text{Diagram: circle with two vertical lines} \right) \Big|_{x \neq 0} \Rightarrow \delta \tilde{p}_3|_{\text{Eq. (7.3)}} = \frac{1}{x} \frac{24 - 12\xi + 5\xi^2}{64} - \frac{5}{24} + \frac{1}{3} \ln 2 + \mathcal{O}(x, \epsilon), \quad (\text{B.7})$$

while

$$\frac{1}{16} \left(\text{Diagram: circle with two vertical lines} \right) \Big|_{x=0} \Rightarrow \delta \tilde{p}_3|_{\text{Eq. (7.2)}} = -\frac{5}{24} + \frac{1}{3} \ln 2 + \mathcal{O}(\epsilon). \quad (\text{B.8})$$

Again, the $1/x$ -divergences of the type in Eq. (B.7) cancel when gluon rings with all possible 1-loop scalar insertions are summed together.

As a comparison of Eqs. (B.4) and (B.6), or Eqs. (B.7) and (B.8) shows, the computation carried out with an IR cutoff leads in general to a more pronounced gauge-parameter dependence for single graphs than the computation carried out according to Eq. (7.2), just because the introduction of a mass according to Eq. (B.1) breaks gauge invariance. The results of Eqs. (B.6), (B.8) are anomalously simple, however: in general there is certainly gauge-parameter dependence left over in single graphs also with the procedure of Eq. (7.2). For example,

$$\frac{1}{8} \left(\text{Diagram: circle with a wavy line and a vertical line} \right) \Big|_{x=0} \Rightarrow \delta \tilde{p}_3|_{\text{Eq. (7.2)}} = \frac{1}{32\epsilon} (13 - 4\xi + \xi^2) + \frac{40 - 28\xi + 5\xi^2}{32} + \mathcal{O}(\epsilon), \quad (\text{B.9})$$

and ξ cancels only in the sum.

⁶The first two terms in Eq. (B.4) can be written as $(2 - 2\xi + \xi^2)[\ln(3x/2) - 1/(4\epsilon)]/8 + 1/(32\epsilon)$, showing that the result of Eq. (B.6) arises after a cancellation of IR and UV divergences in dimensional regularisation.

References

- [1] S. Bronoff, R. Buffa and C.P. Korthals Altes, *Phase diagram of 3D $SU(3)$ gauge-adjoint Higgs system*, hep-ph/9809452; S. Bronoff and C.P. Korthals Altes, *Phase diagram of 3D $SU(3)$ gauge-adjoint Higgs system and C -violation in hot QCD*, Phys. Lett. B 448 (1999) 85 [hep-ph/9811243].
- [2] A. Rajantie, *$SU(5)$ + adjoint Higgs model at finite temperature*, Nucl. Phys. B 501 (1997) 521 [hep-ph/9702255]; K. Kajantie, M. Laine, A. Rajantie, K. Rummukainen and M. Tsypin, *The phase diagram of three-dimensional $SU(3)$ + adjoint Higgs theory*, JHEP 9811 (1998) 011 [hep-lat/9811004].
- [3] E. Braaten and A. Nieto, *Free energy of QCD at high temperature*, Phys. Rev. D 53 (1996) 3421 [hep-ph/9510408].
- [4] K. Kajantie, M. Laine, K. Rummukainen and Y. Schröder, *How to resum long-distance contributions to the QCD pressure?*, Phys. Rev. Lett. 86 (2001) 10 [hep-ph/0007109].
- [5] P. Arnold and C. Zhai, *The three loop free energy for pure gauge QCD*, Phys. Rev. D 50 (1994) 7603 [hep-ph/9408276]; *The three loop free energy for high temperature QED and QCD with fermions*, *ibid.* 51 (1995) 1906 [hep-ph/9410360].
- [6] C. Zhai and B. Kastening, *The free energy of hot gauge theories with fermions through g^5* , Phys. Rev. D 52 (1995) 7232 [hep-ph/9507380].
- [7] K. Kajantie, M. Laine, K. Rummukainen and M. Shaposhnikov, *3d $SU(N)$ + adjoint Higgs theory and finite-temperature QCD*, Nucl. Phys. B 503 (1997) 357 [hep-ph/9704416].
- [8] A.D. Linde, *Infrared problem in thermodynamics of the Yang-Mills gas*, Phys. Lett. B 96 (1980) 289.
- [9] D.J. Gross, R.D. Pisarski and L.G. Yaffe, *QCD and instantons at finite temperature*, Rev. Mod. Phys. 53 (1981) 43.
- [10] P. Ginsparg, *First and second order phase transitions in gauge theories at finite temperature*, Nucl. Phys. B 170 (1980) 388; T. Appelquist and R.D. Pisarski, *High-temperature Yang-Mills theories and three-dimensional Quantum Chromodynamics*, Phys. Rev. D 23 (1981) 2305.
- [11] K. Kajantie, M. Laine, K. Rummukainen and Y. Schröder, *The pressure of hot QCD up to $g^6 \ln(1/g)$* , Phys. Rev. D, in press [hep-ph/0211321].
- [12] Y. Schröder, *Logarithmic divergence in the energy density of the three-dimensional Yang-Mills theory*, in preparation.

- [13] K. Kajantie, M. Laine, K. Rummukainen and Y. Schröder, *Measuring infrared contributions to the QCD pressure*, Nucl. Phys. B (Proc. Suppl.) 106 (2002) 525 [hep-lat/0110122]; *Four-loop logarithms in 3D gauge + Higgs theory*, hep-lat/0209072.
- [14] K. Kajantie, M. Laine and Y. Schröder, *A simple way to generate high order vacuum graphs*, Phys. Rev. D 65 (2002) 045008 [hep-ph/0109100].
- [15] M. Achhammer, *The QCD Partition Function at High Temperatures*, PhD thesis, University of Regensburg, July 2000 (Logos-Verlag, Berlin, 2001).
- [16] Y. Schröder, *Automatic reduction of four-loop bubbles*, Nucl. Phys. B (Proc. Suppl.) 116 (2003) 402 [hep-ph/0211288].
- [17] J.A.M. Vermaseren, *New features of FORM*, math-ph/0010025; <http://www.nikhef.nl/~form/>.
- [18] K.G. Chetyrkin and F.V. Tkachov, *Integration by parts: the algorithm to calculate beta functions in 4 loops*, Nucl. Phys. B 192 (1981) 159; F.V. Tkachov, *A theorem on analytical calculability of four loop renormalization group functions*, Phys. Lett. B 100 (1981) 65.
- [19] S. Laporta, *High-precision calculation of multi-loop Feynman integrals by difference equations*, Int. J. Mod. Phys. A 15 (2000) 5087 [hep-ph/0102033].
- [20] D.J. Broadhurst, *Three loop on-shell charge renormalization without integration: $\Lambda_{\overline{MS} QED}$ to four loops*, Z. Phys. C 54 (1992) 599.
- [21] K. Farakos, K. Kajantie, K. Rummukainen and M. Shaposhnikov, *3d physics and the electroweak phase transition: a framework for lattice Monte Carlo analysis*, Nucl. Phys. B 442 (1995) 317 [hep-lat/9412091].
- [22] M. Laine and A. Rajantie, *Lattice-continuum relations for 3d SU(N)+Higgs theories*, Nucl. Phys. B 513 (1998) 471 [hep-lat/9705003].
- [23] S.A. Larin and J.A.M. Vermaseren, *The three loop QCD beta function and anomalous dimensions*, Phys. Lett. B 303 (1993) 334 [hep-ph/9302208]; S.A. Larin, F.V. Tkachov and J.A.M. Vermaseren, *The FORM version of Mincer*, preprint NIKHEF-H-91-18.
- [24] E. Braaten and A. Nieto, *Effective field theory approach to high temperature thermodynamics*, Phys. Rev. D 51 (1995) 6990 [hep-ph/9501375].
- [25] A. Vuorinen, *Quark number susceptibilities of hot QCD up to $g^6 \ln(g)$* , Phys. Rev. D, in press [hep-ph/0212283].
- [26] J.P. Blaizot, E. Iancu and A. Rebhan, *On the apparent convergence of perturbative QCD at high temperature*, hep-ph/0303045.

- [27] G. Cvetič and R. Kögerler, *Resummations of free energy at high temperature*, Phys. Rev. D 66 (2002) 105009 [hep-ph/0207291].
- [28] M. Strickland, *Reorganizing finite temperature field theory*, Int. J. Mod. Phys. A 16S1C (2001) 1277; E. Braaten, *Thermodynamics of hot QCD*, Nucl. Phys. A 702 (2002) 13; A. Peshier, *Resummation of the QCD thermodynamic potential*, Nucl. Phys. A 702 (2002) 128 [hep-ph/0110342]; J.O. Andersen, *Hard thermal loops and QCD thermodynamics*, hep-ph/0210195; J.P. Blaizot, E. Iancu and A. Rebhan, *Thermodynamics of the high-temperature quark gluon plasma*, hep-ph/0303185.
- [29] K. Farakos, K. Kajantie, K. Rummukainen and M.E. Shaposhnikov, *3d physics and the electroweak phase transition: perturbation theory*, Nucl. Phys. B 425 (1994) 67 [hep-ph/9404201].
- [30] P.N. Tan, B. Tekin and Y. Hosotani, *Maxwell-Chern-Simons scalar electrodynamics at two loops*, Nucl. Phys. B 502 (1997) 483 [hep-th/9703121].
- [31] J.O. Andersen, *3d effective field theory for finite temperature scalar electrodynamics*, Phys. Rev. D 59 (1999) 065015 [hep-ph/9709418].
- [32] K. Kajantie, M. Karjalainen, M. Laine and J. Peisa, *Three-dimensional $U(1)$ gauge + Higgs theory as an effective theory for finite temperature phase transitions*, Nucl. Phys. B 520 (1998) 345 [hep-lat/9711048].
- [33] B. Kastening, H. Kleinert and B. Van den Bossche, *Three-loop ground-state energy of $O(N)$ -symmetric Ginzburg-Landau theory above T_c in $4-\epsilon$ dimensions with minimal subtraction*, Phys. Rev. B 65 (2002) 174512 [cond-mat/0109372].
- [34] S. Laporta, *High-precision ϵ -expansions of massive four-loop vacuum bubbles*, Phys. Lett. B 549 (2002) 115 [hep-ph/0210336].
- [35] A. Devoto and D.W. Duke, *Table of integrals and formulae for Feynman diagram calculations*, Riv. Nuovo Cim. 7N6 (1984) 1.
- [36] A. Vuorinen, *Four-loop Feynman diagrams in three dimensions*, Master's Thesis, Helsinki University, 2001 (unpublished) [<http://ethesis.helsinki.fi/julkaisut/mat/fysii/pg/vuorinen/fourloop.pdf>].
- [37] S. Groote, J.G. Korner and A.A. Pivovarov, *Configuration space based recurrence relations for sunset-type diagrams*, Eur. Phys. J. C 11 (1999) 279 [hep-ph/9903412].
- [38] A.K. Rajantie, *Feynman diagrams to three loops in three-dimensional field theory*, Nucl. Phys. B 480 (1996) 729; *ibid.* B 513 (1996) 761 (E) [hep-ph/9606216].